arXiv:2609.27490v2 [cs.AI] 28 Sep 2026

WHATWORKEDBENCH: BENCHMARKING EXPERIMENTAL UNDERSTANDING IN AI AGENTS

Jingjie Ning[1]* **Xueqi Li**[1] **Yibo Kong**[1] **Dongting Li**[2]

[1]Carnegie Mellon University [2]Tsinghua University

{jening, xueqil, yibok}@cs.cmu.edu ldt25@mails.tsinghua.edu.cn

Homepage GitHub

ABSTRACT

AI research agents must predict the effects of computational changes after budgeted experiments. WhatWorkedBench evaluates this *experimental understanding* through a delivered *response surface* of configuration scores. Agents inspect workflow code and buy measurements; exhaustive CPU references score conditional component effects, mean pair interactions, configuration choice, and delivery. The catalog spans 36 task conditions, 30 sources, 8 workflow families, and 1248 indexed configuration records, with 4,206 numerical controls. At eight purchased measurements plus two free anchors, pair-effect ridge selects an exact optimum on 15 of 22 sources; 13 of these cases have at least one conditional-effect error exceeding 10% of the task utility range. Shared-estimator comparisons measure acquisition and reconstruction on common observations. In a prospective typed study on 12 four-factor sources, DeepSeek Flash submits 12/12 direct tables and gains 0.147 recovery over a Gaussian process (GP) fitted to the same observations. Pro delivers 11/12 artifacts, with an all-attempt GP difference of -0.001 and a delivered-only difference of $+0.063$. On six prespecified new agent-evaluation sources, Flash and Pro gains are 0.149 and 0.074. In eight typed six-factor episodes, seven final tables satisfy verified code equivalences. Four fresh agents pass all six registered rules through named estimators and deliver consistent tables at 0.682 recovery versus 0.710 for separate direct-table runs. WhatWorkedBench links acquisition, inference, program structure, and delivery.

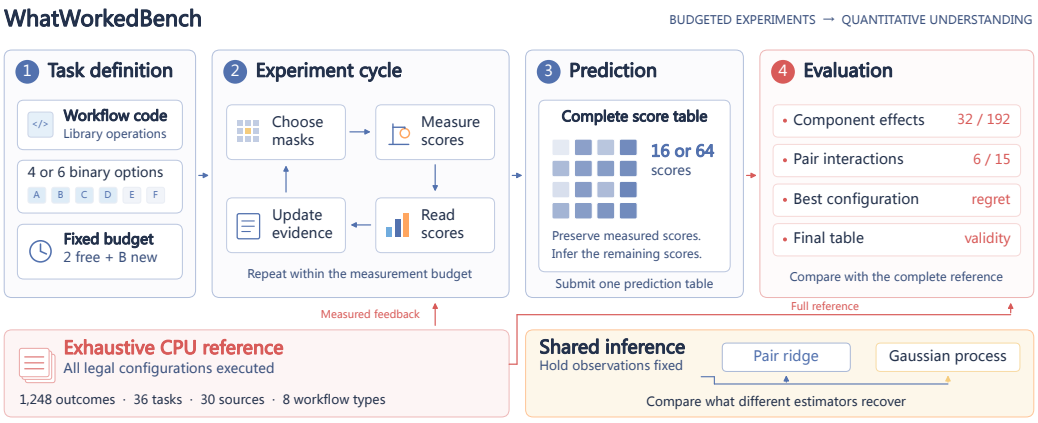

Figure 1: WhatWorkedBench connects budgeted experiments to quantitative understanding. Agents inspect a workflow, query selected configurations, and submit a complete prediction table. The evaluator uses exhaustive CPU outcomes to score conditional effects, mean pair interactions (departures from additive effects), configuration choice, and artifact delivery. Shared inference compares estimators on the same observations.

*Corresponding author

1 INTRODUCTION

AI agents increasingly plan, execute, and interpret computational experiments (Huang et al., 2024; Chan et al., 2025; Kon et al., 2026). Research agents use trial histories to revise training recipes and carry lessons from cheap experiments to costly configurations (Ning et al., 2026a; Guo et al., 2026). Reliable experimentation requires predicting how component changes behave in new settings and combine with other changes. Measuring this acquired knowledge is central to evaluating systems that learn through experimentation.

We study *experimental understanding* as the accuracy of quantitative predictions about computational interventions available at the end of an experimental episode. The evaluated system combines an agent's measurement policy, numerical tools, and submitted prediction artifact. A *native outcome* is the score of a code-option intervention with source data, implementation, and evaluation cohort fixed. An agent inspects workflow code and component definitions, chooses experiments under a measurement budget, and submits a complete predicted response surface (Figure 1). A *background* fixes the settings of every other component. The reference evaluates each component's effect in every background. These conditional effects describe arbitrary combinations of the documented interventions. They connect the experiments an agent chooses to the predictive knowledge that its final artifact contains.

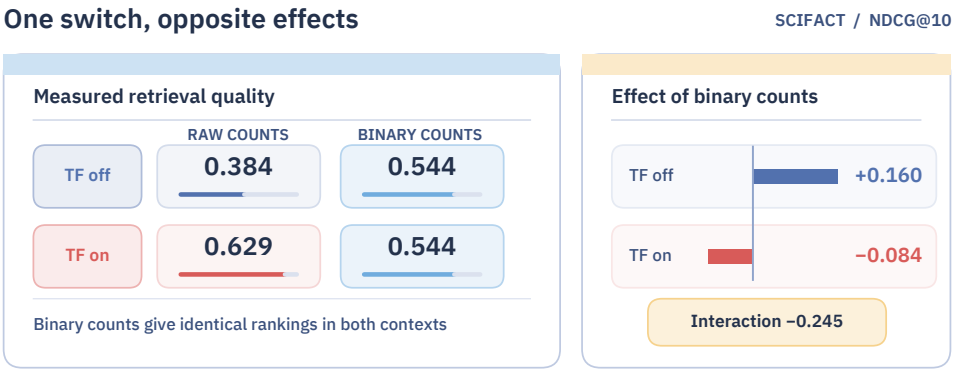

Figure 2: A retrieval switch reverses its effect across two workflow backgrounds. The left panel reports SciFact normalized discounted cumulative gain at rank 10 (NDCG@10) for raw and binary term counts with sublinear term frequency (TF) off or on. The right panel shows that binary counts raise NDCG@10 by 0.160 with TF off and lower it by 0.084 with TF on, yielding a -0.245 interaction. Binary counts make the sublinear transform inactive, so both right-column cells have identical rankings and score 0.544. Other settings use unigrams, English stopword removal, disabled inverse document frequency, and unnormalized vectors.

Figure 2 illustrates why the full intervention context matters. The same retrieval option improves one configuration and degrades another. This dependence of one change on another is an *interaction*. Across the catalog, 20 of 30 distinct sources, representing 24 of 36 indexed task conditions, contain a sign reversal with positive and negative effects each exceeding 5% of the response range; At a 10^{-12} numerical floor, 35 of 36 conditions and 29 of 30 sources contain a reversal. A single preferred configuration or an average component effect leaves these conditional behaviors unresolved. WhatWorkedBench makes them explicit quantitative prediction targets.

The benchmark connects three algorithmic decisions. *Measurement selection* determines which evidence is acquired. *Numerical inference* predicts unmeasured outcomes from that evidence. *Program structure* supplies relations among configurations, including inactive options. A *shared-estimator cross-comparison* fits one estimator to observations from different acquisition policies and fits different estimators to fixed observations. Each contrast holds one part of the executable task fixed and tracks how recovery changes with the other.

- We define an executable evaluation of experimental understanding through complete conditional component effects. The reference covers arbitrary combinations of each task's documented changes, alongside configuration choice and final artifact delivery.
- We provide 36 task conditions on 30 sources across 8 computational workflow families. Exhaustive native execution yields 1248 indexed configuration records (1,152 distinct source–configuration outcomes), 3,392 indexed conditional effects (including 192 paired-subcube repeats), and 342 mean pair interactions, with standalone execution and grading.
- Across 4,206 numerical controls, 108 core agent episodes, and 24 typed episodes on 12 sources, we measure acquisition, numerical inference, program structure, and delivery. Across all 12 typed sources, Flash gains 0.147 recovery over the same-observation GP; Pro has an all-attempt difference of -0.001 and a delivered-only difference of $+0.063$. Six new sources yield Flash and Pro gains of 0.149 and 0.074. Separate diagnostics trace code-derived rules into final tables.

2 Related Work

Interactive discovery. ScienceWorld and DiscoveryWorld assess scientific reasoning in interactive environments (Wang et al., 2022; Jansen et al., 2024). CausalGame evaluates experimental design and causal explanations under hidden confounding (Chen et al., 2026). Table 1 maps nearby benchmarks to their experimental settings and scored artifacts.

Table 1: Experimental settings and scored artifacts in nearby evaluations.

Benchmark	Setting and scored artifact
BoxingGym (2025)	Scientific worlds; experiment choice and prediction
Gravity-Bench (2025)	Gravity simulations; numerical discovery answers
Science-Gym (2026); SciGym (2025)	Physics and biology; equations and system reconstruction
Science sandboxes (2026)	Biological loops; optimization and scientific understanding
CAFE (2026)	Compound-AI pipelines; factorial effects and interactions
petri-bench (n.d.)	Perturbed simulations; changed factors and interaction signs
AstaBench (2026)	Research workflows; artifacts and task outcomes
WhatWorkedBench	Budgeted native workflows; complete score tables and conditional effects

Research workflows. AbGen, AblationBench, and SCOPE assess experiment plans (Zhao et al., 2025; Abramovich and Chechik, 2025; Liu et al., 2026b). MLAgentBench, MLE-bench, BLADE, ScienceAgentBench, EXP-Bench, and ResearchGym evaluate executable research outcomes (Huang et al., 2024; Chan et al., 2025; Gu et al., 2024; Chen et al., 2025; Kon et al., 2026; Garikaparthi et al., 2026). FIRE-Bench scores rediscovered findings; AgentActionBench scores reproduction traces (Wang et al., 2026; Hong et al., 2026).

Experimental design. Factorial design and computer experiments study component effects and response prediction (Box et al., 2005; Sacks et al., 1989). Hyperparameter optimization studies conditional search and GP-guided acquisition (Bergstra et al., 2011; Lindauer et al., 2022; Snoek et al., 2012); fANOVA summarizes variation over configuration distributions (Hutter et al., 2014). Our complete response surfaces score conditional effects and mean pair interactions after budgeted measurements. Shared-observation comparisons connect this evaluation to Bayesian experimental design (Chaloner and Verdinelli, 1995; Rainforth et al., 2024). Appendix A expands the comparison.

3 Task and evaluation protocol

For task t, native execution defines a deterministic utility $u_t(z) \in [0,1]$ on configurations $z \in \{0,1\}^{d_t}$, with $d_t \in \{4,6\}$. Each bit is a binary option, called a *factor*; the full vector is a *mask*. All masks are legal. The agent receives two free anchor measurements, $u_t(0^{d_t})$ and $u_t(1^{d_t})$, and may purchase at most B additional distinct measurements. It can query adaptively or in batches.

Repeated measurements are free and over-budget batches are rejected atomically. Each utility table is defined by the case's frozen algorithm implementation, random seed, and evaluation cohort. Four- and six-factor designs permit exhaustive, independently replayed references while varying how much of the response surface a budget reveals.

The final artifact is a prediction $\hat{u}_t(z)$ for every legal mask, with finite values in $[0, 1]$. Grading inserts authoritative observations at measured cells. Submission closes the episode and establishes the delivered artifact used for the final score. The protocol records intermediate calculations as part of the experimental trajectory. Measured endpoint pairs give exact effects; the remaining contrasts require predictions at one or both endpoints. Appendix F.6 reports coverage and prediction error.

Primary numerical target. For component i and background z with $z_i = 0$, define

$$\Delta_i(z) = u_t(z + e_i) - u_t(z), \qquad E_t = \frac{1}{d_t 2^{d_t-1}} \sum_i \sum_{\substack{z \in \{0,1\}^{d_t} \\ z_i = 0}} |\widehat{\Delta}_i(z) - \Delta_i(z)|. \tag{1}$$

These effects describe every joint intervention. For configurations x, y, a path that switches their differing bits gives

$$u_t(y) - u_t(x) = \sum_{e \in \mathrm{path}(x,y)} s_e \Delta_e, \qquad s_e \in \{-1, 1\}. \tag{2}$$

Thus complete conditional effects and one anchor determine the whole response surface. Deriving all predicted effects from a single submitted table preserves this path consistency. If every conditional-effect error is at most ϵ, the error of any k-component intervention is at most $k\epsilon$. Appendix F gives the derivation and a configuration-choice counterexample that clarifies the need for an effect-based evaluation target.

There are 32 conditional effects at four factors and 192 at six. Let A_t be the mean absolute true conditional effect. We report raw effect MAE E_t and relative recovery $R_t = \max(0, 1 - E_t/A_t)$ for $A_t > 10^{-12}$. For a numerically flat table, recovery is one only when $E_t \leq 10^{-12}$. A zero recovery score corresponds to error at least as large as the mean true-effect magnitude. Reporting E_t, A_t, and the utility range preserves the numerical scale of each reconstruction problem.

Additional numerical outputs. For every pair of components, we additionally compare the mean second difference $u(z + e_i + e_j) - u(z + e_i) - u(z + e_j) + u(z)$, averaging over the remaining backgrounds. These averages summarize pair interactions; the complete conditional effects retain their dependence on other components. We report MAE over the six or 15 pair contrasts, together with grid MAE and selection regret $\max_z u_t(z) - u_t(\arg\max_z \hat{u}_t(z))$. Prediction ties prefer fewer enabled options and then the lexically smaller mask. Exact optimality allows regret up to 10^{-12}.

The strict reconstruction score requires every conditional-effect error to be at most $\max[10^{-12}, \tau(\max u_t - \min u_t)]$. We set the development tolerance to $\tau = 0.1$ and evaluate a five-tolerance profile alongside continuous recovery. Missing delivery receives zero recovery and a strict score of zero. Raw errors include valid artifacts with explicit sample counts.

4 Native catalog and reference validation

A *source* is a dataset or record; a *task condition* pairs a source with a set of workflow options. A *family* groups tasks by computation and metric. Table 2 summarizes the catalog. The four-factor track contains 22 instances. A paired track adds two options on one source per family, producing six six-factor variants. The six-factor track additionally includes four beat-detection records and four graph instances. Thus there are 36 task conditions on 30 sources, comprising 352 four-factor and 896 six-factor configuration records. Of these, 96 reproduce original subcube outcomes.

The catalog combines predictive learning, partition discovery, temporal prediction, signal and image processing, and ranked retrieval. Its options change representations, estimators, preprocessing, or computational operators. Every outcome is produced by the documented native-library workflow on source data. The source inventory, preparation, and all 48 workflow options appear in Appendices B–D. Each task records its source, implementation, random seed, and evaluation cohort. Construction plans specify the additional sources and configurations before their execution.

Table 2: Task conditions and source inventory. Paired variants share their original sources. Source metadata retain dataset and library relationships, including the classifier reused for link prediction.

Workflow	$d = 4$	$d = 6$	Sources	Native operation and metric
Classification	4	1	4	Logistic regression; balanced accuracy
Regression	4	1	4	Ridge regression; transformed MAE
Clustering	4	1	4	k-means; normalized mutual information
Forecasting	4	1	4	One-step ridge forecasts; transformed MAE
Restoration	4	1	4	Native image filters; transformed pixel RMSE
Retrieval	2	1	2	TF–IDF retrieval; NDCG@10
Beat detection	0	4	4	SciPy signal processing; event F1
Link prediction	0	4	4	NetworkX features and logistic regression; ROC AUC
Total	22	14	30	36 conditions across eight families

Conditional structure across the catalog. Figure 3 shows how one code option changes task utility across two backgrounds in image restoration, beat detection, and link prediction. Across the catalog, 24 of 36 conditions contain a sign reversal with both directions above 5% of the response range. The 10^{-12} numerical floor yields 35 conditions; 1% and 10% floors yield 33 and 16. Flat exports provide all 3,392 conditional effects and 342 mean pair interactions for reuse.

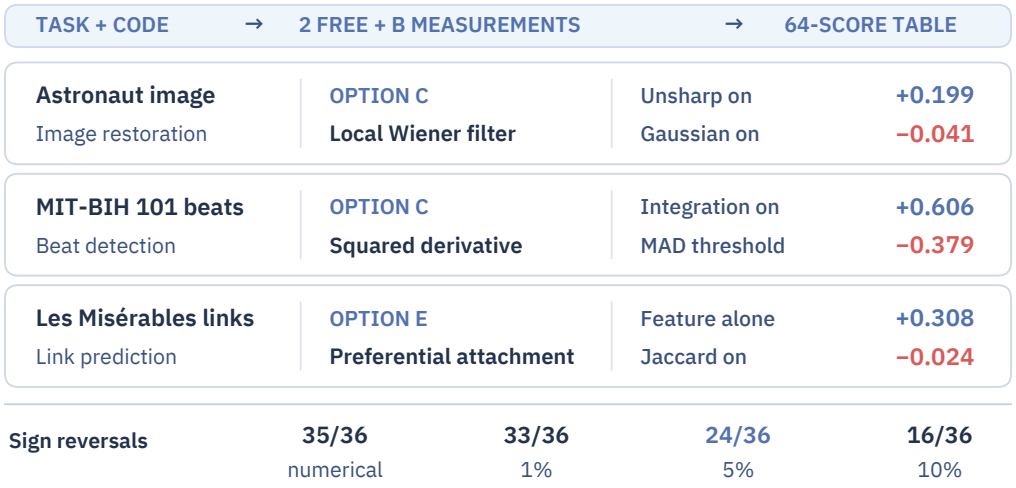

Figure 3: Native conditional effects in three six-option tasks. Each row changes one documented code option while fixing all other options in two backgrounds. Values are evaluator-known changes in normalized task utility. The top strip shows two free anchors, a budget of B purchased outcomes, and a 64-score final table. The bottom strip counts sign reversals over all 36 task conditions at the indicated effect floors.

Data access and native evaluation. Training partitions fit supervised transforms and models, while feature-identical rows remain grouped across splits. Clustering labels enter the external metric. Forecasts use preceding observations with parameters fitted on the training prefix. Restoration retains clean references at the evaluator, and retrieval uses original relevance annotations with query-copy exclusion for ArguAna. Beat detection uses archived MIT-BIH waveforms and event annotations (Moody and Mark, 2001; Pollard et al., 2026). Link prediction computes features on an observed graph, fits calibration labels, and evaluates disjoint test pairs. Appendix C specifies access rules and scoring cohorts.

Complete references and reproducible episodes. Cold execution checks all configuration predictions against their recorded hashes. Separately implemented native metrics and target-perturbation checks verify the scoring and evaluation boundaries. The prepared-input pack replays all 1248

records from the prepared-input archive in 127.87 seconds with one computation thread. The standalone episode engine agrees with 4206 stored numerical-control records. These checks establish a common reference for repeated evaluation.

An *information budget* caps purchased outcomes. Agents view public tasks and cached feedback; the evaluator retains complete references for matched policy comparisons.

5 EXPERIMENTAL SETUP

Shared-estimator cross-comparison. For task t, acquisition policy π produces an observation set $O_{t,\pi}$. Let $\mathcal{R}_t(\pi, g)$ denote effect recovery when estimator g fits those observations. With g fixed, contrasts across policies compare acquired observation sets. With $O_{t,\pi}$ fixed, contrasts across estimators compare reconstruction rules.

Numerical reference methods. Main-effect ridge (D1) models additive component contributions; pair-effect ridge (D2) additionally models pairwise interactions. Sequential ridge designs spread measurements over these component features. Random design uses 20 seeds with the pair estimator. A Gaussian-process baseline estimates a constant mean and models similarity through the number of differing options (Rasmussen and Williams, 2006). Regularization and kernel parameters minimize leave-one-out prediction error on observed values. Grid GP and Effect GP select measurements to reduce uncertainty in scores and conditional effects, respectively (Cohn et al., 1996). All predictors retain measured values. Appendix G gives the feature maps, covariance, and acquisition criteria.

We additionally evaluate public-code equivalences for the original six-factor variants. For example, a filter-width option is inactive when its filter is off. An *equivalence class* contains configurations with identical native behavior. The control measures one representative per class and assigns its prediction to every class member. The trajectory records purchased measurements and inferred aliases separately. Every equivalence is checked against native prediction hashes and scores. Ridge controls, GP controls, and code-equivalence controls follow recorded development stages. The protocol history and exact method grids appear in Appendix J.

Agents and budgets. Numerical controls cover all eight workflow families. The 108-episode core agent study uses Spambase, Concrete, Wine, CO_2, Astronaut, and SciFact, the six one-per-family sources frozen with the initial four-factor agent study. Matched controls use these same sources. Four-factor evaluation uses the API identifiers `deepseek-v4-flash` and `deepseek-v4-pro` at $B = 4, 8$ for 72 episodes across the original and additional cohorts. We abbreviate these identifiers as Flash and Pro. Both identifiers belong to one DeepSeek model family. The evaluated tasks use binary switches in CPU-executable workflows. Both models receive workflow code and input summaries, reasoning enabled at high effort, a 32,768-token output cap, and a disclosed 1,800-second session deadline. The four tools expose current evidence, purchase masks, execute numerical Python, and register a final prediction artifact. A maximum of 20 calculation calls applies, with 30 CPU seconds and 45 wall seconds per call. NumPy, SciPy, scikit-learn, and public main-effect and pair-effect ridge helpers are available.

The information study contains 36 Flash episodes at $B = 20$ on six paired six-factor workflows. Full-code and opaque views share tools, helpers, and utility receipts; the full view adds code and factor semantics. Four-factor evaluation contains three executions per source, model identifier, and budget across dated cohorts. The $B = 32$ beat-detection and graph extension contains eight Flash attempts and six delivered tables. Exact prompts, source pairs, and chronology appear in Appendices H–J.

Artifact-interface diagnostics. An *artifact interface* receives a complete mask-to-utility table or a request to fit a named estimator. Four six-factor sources with verified code equivalences receive matched Flash episodes at $B = 20$ under a typed table argument. Both arms accept complete objects and report rules before measurement; the menu adds GP and agent-supplied estimator rules to ridge fitting. A fresh inference diagnostic holds each ridge-arm episode's 22 observations fixed and requires a named estimator with submitted rules. Exact contracts and results appear in Appendix K.4.

Prospective source cohort. A typed-interface study pairs Flash and Pro at $B = 8$ on 12 four-factor sources. The frozen plan selects the alphabetically first agent-unevaluated source ID in each original family and retains the six core sources. Both models receive identical public tasks and can submit tables or invoke ridge and GP helpers. Source-paired comparisons fit a common GP to agent-purchased observations and frozen D2 observations. The GP uses purchased masks and utilities; agent tables may also encode public workflow code and sandbox calculations. The $R_{\mathrm{all}} - R_{\mathrm{GP}}$ contrast measures final-prediction gain over a fixed numerical baseline at the same purchased masks. Delivery, all-attempt recovery, and delivered-table recovery remain separate (Appendix K.5).

Aggregation and delivery. Numerical controls and core cohorts average repetitions within source, sources within family, and then weight families equally. We call this *family-macro averaging*. The prospective cohort averages sources equally; R_{del} averages delivered sources; bootstrap ranges resample sources. Masks and random seeds remain repeated observations within a source. Four-factor evaluation delivers 63 of 72 artifacts. Every attempt retains its delivery status, and missing delivery receives zero all-attempt recovery. Appendix J gives transport accounting, and Appendix K reports all core episode outcomes.

6 Results

6.1 Optimization success and intervention knowledge are distinct targets

Exact configuration choice can coexist with arbitrarily small effect recovery, even when both free anchors match. Appendix F gives a compact construction. Native measurements show how the two targets separate in practice.

Figure 4 compares recovery across budgets. On the 22 four-factor sources, pair-effect design/ridge at $B = 8$ achieves 0.612 family-macro recovery, 15 exact configuration choices, and three strict reconstructions. Thirteen instances combine exact choice with an effect error above the strict tolerance. The effect-variance GP reaches 0.701 recovery, 16 exact choices, and one strict reconstruction at $\tau = 0.1$. The 13 pair-ridge instances that combine exact choice with a strict-effect error, together with the construction in Appendix F, establish configuration choice and conditional-effect accuracy as complementary evaluation targets.

Appendix L reports the complete strict-error tolerance profile alongside native-unit results.

6.2 Acquisition and estimator contrasts on common observations

At $B = 8$, Flash delivers recovery 0.632 and 0.621 across the original and additional cohorts. Pro delivers 4/6 and 9/12 artifacts, with delivered-table recovery 0.549 and 0.671. Among 18 Flash episodes, seven select an exact optimum and one passes strict reconstruction. Pair ridge scores 0.627 on the same six sources. Appendix Table 6 separates every cohort's delivery, all-attempt recovery, delivered recovery, and shared-GP fit.

At $B = 8$, 32.6% of original Flash effect edges have both endpoints measured; 67.4% require prediction. Filling unmeasured utilities with the observation mean gives normalized error 1.054 on these edges and recovery 0.287, versus 0.542 and 0.632 for delivered tables. The additional Flash cohort recovers 0.621 versus 0.213 for mean completion (Appendix F.6).

All 94 valid core final artifacts select public ridge helpers, with 77 pair-effect and 17 main-effect selections. Both helpers use the same leave-one-out regularization grid as the shared D1 and D2 fits. Each table equals its selected shared fit. At $B = 8$, Flash selects D1/D2 in 2/10 original and 2/4 additional episodes; the selected fit has higher same-observation recovery in 7/12 and 5/6 episodes, respectively. Table 3 crosses acquisition policies with common D1, D2, and GP estimators

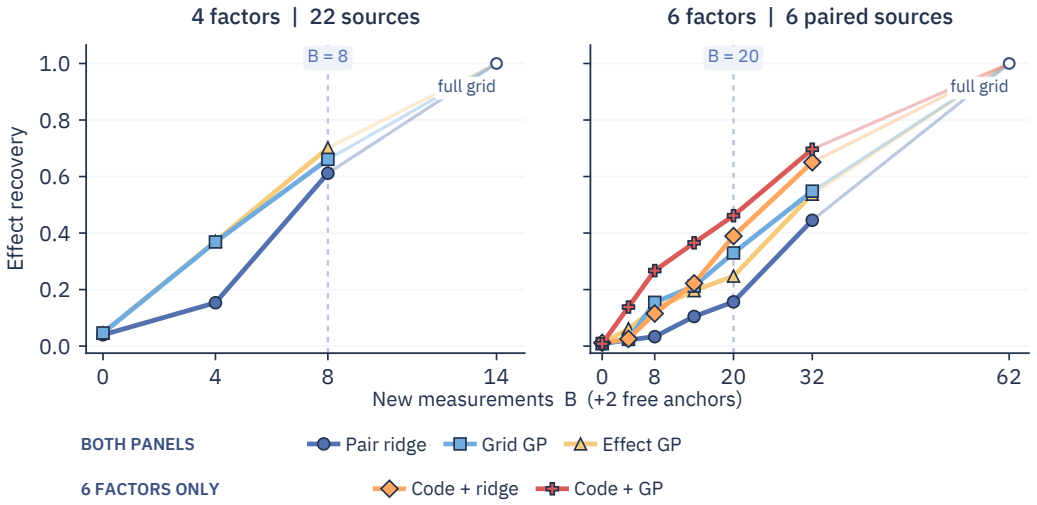

Figure 4: Family-macro conditional-effect recovery across measurement budgets. The left panel contains 22 four-factor sources; the right panel contains six paired six-factor sources. Vertical guides mark the $B = 8$ and $B = 20$ comparison budgets. Pale final segments end at complete configuration enumeration, with $B = 14$ and $B = 62$. Code-equivalence methods appear only on the six-factor track and encode visible inactive-parameter rules.

at $B = 8$ on the same six sources. Point estimates reorder policies across estimators. Original Flash observations yield 0.698 recovery with the shared GP versus 0.669 for D2 observations; under shared D2, the values are 0.550 and 0.627. The additional Flash cohort repeats this pattern with 0.720 versus 0.669 under GP and 0.537 versus 0.627 under D2. The pooled Flash-minus-D2 acquisition contrast under this GP is $+0.040$ (descriptive interval $[-0.039, 0.132]$; four of six sources positive). The source-level paired contrasts appear in Appendix L.1.

Table 3: Core-cohort acquisition and reconstruction at $B = 8$ on six matched four-factor sources. Rows fix an acquisition policy; shared columns fit each estimator to that policy's observations. Random designs average 20 seeds within source. R_{all} assigns zero to missing artifacts, and shared fits use all acquired evidence.

Acquisition	Records	R_{all}	Shared D1	Shared D2	Shared GP
Flash, original	12	0.632	0.604	0.550	0.698
Pro, original	6	0.366	0.628	0.567	0.692
Flash, additional	6	0.621	0.598	0.537	0.720
Pro, additional	12	0.503	0.564	0.670	0.667
D1	6	0.546	0.546	0.592	0.592
D2	6	0.627	0.571	0.627	0.669
Random D2	120	0.523	0.542	0.523	0.619
GP-G	6	0.666	0.564	0.633	0.666
GP-E	6	0.640	0.553	0.568	0.640

Prospective inference across 12 sources. Table 3 records selected core ridge fits. The typed cohort in Table 4 has a distinct prompt, execution date, and direct-table contract. On the six recurring sources, the shared-GP Flash-minus-D2 acquisition point estimates are $+0.040$ in core and -0.051 in typed runs. Flash submits 12 direct tables and exceeds the same-observation GP on 11/12 sources, with mean $R_{\text{all}} - R_{\text{GP}} = +0.147$. Pro delivers 11/12 artifacts. Its all-attempt contrast is -0.001; among delivered artifacts, its mean contrast with the GP on those same 11 sources is $+0.063$. The prespecified six-source new subgroup yields positive table-minus-GP contrasts on 6/6 Flash sources and 4/6 Pro sources, with one Pro tie and one negative contrast. Pro selects the named GP on

Table 4: Typed cohort on six new and six original sources at $B = 8$. R_{all} scores absent submissions as zero; R_{del} averages delivered tables. R_{GP} uses the same observations. Gain is $R_{\text{all}} - R_{\text{GP}}$. Ranges give descriptive 2.5th–97.5th source-bootstrap percentiles.

Sources	Model	Valid	R_{all}	R_{del}	R_{GP}	Gain	Range
New	Flash	6/6	0.869	0.869	0.719	$+0.149$	$[0.067, 0.241]$
New	Pro	6/6	0.792	0.792	0.718	$+0.074$	$[0.006, 0.160]$
Original	Flash	6/6	0.764	0.764	0.618	$+0.146$	$[-0.005, 0.360]$
Original	Pro	5/6	0.590	0.708	0.666	-0.076	$[-0.392, 0.215]$
All	Flash	12/12	0.816	0.816	0.669	$+0.147$	$[0.055, 0.261]$
All	Pro	11/12	0.691	0.754	0.692	-0.001	$[-0.177, 0.153]$

A post-hoc oracle using the full reference selects the best same-observation D1, D2, or GP fit per source. Flash retains gains of 0.114 on new sources (6/6 positive) and 0.095 overall (10/12 positive).

Coffee, giving an exact tie. With shared GP, agent-minus-D2 acquisition point estimates for (Flash, Pro) are $(-0.024, -0.026)$ on new sources and $(-0.037, -0.014)$ across all 12. The reported six- and twelve-source bootstrap ranges span zero (Appendix K.5).

6.3 Program rules and final predictions

Across four code-visible sources, the typed arms deliver 8/8 direct tables; seven satisfy every verified equivalence. The four paired menu-minus-ridge recovery contrasts average -0.092, with one positive and three negative sources. Table 5 tracks rule reporting and final artifacts.

Table 5: Rule reporting and final artifacts on four six-factor sources. Rules passed counts registered relations supplied to a named estimator in the final submission call; direct-table submissions pass none. Clean tables satisfy all verified equivalences.

Study	Delivered	First rules	Final mode	Rules passed to named estimator	Clean	Recovery
Typed ridge	4/4	6/6	4 direct	0	3/4	0.710
Typed menu	4/4	6/6	4 direct	0	4/4	0.617
Fixed observations	4/4	6/6	3 GP, 1 D1	6/6	4/4	0.682

Four fresh agents pass all six rules to named estimators; all 96 equivalent pairs agree. Their mean recovery is 0.682 versus 0.710 for the separate typed direct-table arms. On fixed ridge-arm observations, verified rules raise D2 recovery from 0.319 to 0.601 and GP recovery from 0.509 to 0.666 (Appendix K.4). The six-workflow controls jointly apply class-aware acquisition and prediction (Appendices G.3 and L.4). In a separate eight-episode rule-reporting diagnostic, agents identify all registered code relations. Their ridge-helper tables show native-equivalence violations. A class-consistent control scores 0.507 versus 0.338 for the delivered tables (Appendix K.3).

7 Conclusion

WhatWorkedBench grades budgeted response surfaces against exhaustive CPU references for conditional effects, pair interactions, configuration choice, and delivery. Its 36 conditions span 30 sources and 8 workflow families, with 1248 indexed configuration records and 4,206 numerical controls. At eight purchases, pair-effect ridge selects the exact optimum yet exceeds the $\tau = 0.1$ strict effect-error tolerance on 13 of 22 four-factor sources. Shared-estimator comparisons report acquisition and reconstruction on common observations. In the 12-source typed study of DeepSeek Flash and Pro, 23/24 episodes deliver final artifacts. Flash gains 0.147 recovery over the same-observation GP across all 12 sources; Pro has a -0.001 all-attempt contrast and a $+0.063$ delivered-only contrast. Six new sources yield Flash and Pro gains of 0.149 and 0.074. Seven of eight typed six-factor tables satisfy verified equivalences. Four fresh agents deliver rule-consistent tables.

REPRODUCIBILITY STATEMENT

The public benchmark repository is available at `https://github.com/EthanNing/WhatWorkedBench`. It includes public tasks, evaluator-only references, versioned episode semantics, exact native operations, prepared inputs, numerical controls, and machine-readable audits. The task pack's standard-library engine reproduces 4206 stored score records in a standalone process. The prepared-input pack reproduces all 1248 native records from the public repository. Source acquisition and preparation retain separate manifests and code identities.

AI USE STATEMENT

An AI coding assistant contributed to topic and literature exploration, workflow-option design, experiment protocols, data preparation, implementation, numerical analysis, figures, and drafting. DeepSeek models were additionally used as evaluated experimental agents. Verification used cold native replay, separately implemented numerical metrics, and recorded source and code identities. The study preserves the generated implementations, analysis scripts, experiment plans, and numerical audit results.

ETHICS STATEMENT

This work uses publicly available research archives with their accompanying source terms and citations. The ECG tasks evaluate computational event detection on archived waveforms. Prepared inputs contain the signal data and reference events used for scoring. Evaluation references are held by the trusted host, and agents receive task descriptions and budgeted aggregate observations.

REFERENCES

Talor Abramovich and Gal Chechik. AblationBench: Evaluating Automated Planning of Ablations in Empirical AI Research. AI4Science Workshop, ICML, 2026. First preprint 2025. arXiv 2507.08038v3.

James S. Bergstra, Rémi Bardenet, Yoshua Bengio, and Balázs Kégl. Algorithms for Hyper-Parameter Optimization. NeurIPS, 2011. Conference proceedings.

George E. P. Box, J. Stuart Hunter, and William G. Hunter. Statistics for Experimenters: Design, Innovation, and Discovery. Wiley, 2nd edition, 2005. ISBN 978-0-471-71813-0.

Jonathan Bragg et al. AstaBench: Rigorous Benchmarking of AI Agents with a Scientific Research Suite. ICLR, 2026. arXiv 2510.21652.

Mattia Cerrato et al. Science-Gym: a simple testbed for AI-driven scientific discovery. Machine Learning, 115, article 16, 2026. Publisher page.

Kathryn Chaloner and Isabella Verdinelli. Bayesian Experimental Design: A Review. Statistical Science, 10(3):273–304, 1995. Publisher page.

Jun Shern Chan et al. MLE-bench: Evaluating Machine Learning Agents on Machine Learning Engineering. ICLR, 2025. Conference paper.

Abhranil Chandra, Sankaran Vaidyanathan, Utsav Dhanuka, Varun Gandhi, and Scott Niekum. Hierarchical Experimentalist Agents. 2026. arXiv 2606.29315.

Zhenhao Chen, Yongqiang Chen, Chenxi Liu, Junchi Yu, Xiangchen Song, Zijian Li, Jialin Li, Philip Torr, Bo Han, and Kun Zhang. CausalGame: Benchmarking Causal Thinking of LLM Agents in Games. ICML, 2026. arXiv 2607.04293.

Ziru Chen et al. ScienceAgentBench: Toward Rigorous Assessment of Language Agents for Data-Driven Scientific Discovery. ICLR, 2025. arXiv 2410.05080.

João Coelho, Jingjie Ning, Jingyuan He, Kangrui Mao, Abhijay Paladugu, Pranav Setlur, Jiahe Jin, Jamie Callan, João Magalhães, Bruno Martins, and Chenyan Xiong. DeepResearchGym: A Free, Transparent, and Reproducible Sandbox for Deep Research. ICTIR, pp. 34–43, 2026. Publisher page.

David A. Cohn, Zoubin Ghahramani, and Michael I. Jordan. Active Learning with Statistical Models. Journal of Artificial Intelligence Research, 4:129–145, 1996. arXiv cs/9603104.

Haonan Duan et al. Measuring Scientific Capabilities of Language Models with a Systems Biology Dry Lab. 2025. arXiv 2507.02083.

Nicholas Edwards, Yukyung Lee, Yujun Audrey Mao, Yulu Qin, Sebastian Schuster, and Najoung Kim. RExBench: Can coding agents autonomously implement AI research extensions? ACL, 2026. ACL Anthology.

Katharina Eggensperger et al. HPOBench: A Collection of Reproducible Multi-Fidelity Benchmark Problems for HPO. NeurIPS Datasets and Benchmarks, 2021. arXiv 2109.06716.

Adam Foster, Desi R. Ivanova, Ilyas Malik, and Tom Rainforth. Deep Adaptive Design: Amortizing Sequential Bayesian Experimental Design. ICML, pp. 3384–3395, 2021. Conference proceedings.

Kanishk Gandhi et al. BoxingGym: Benchmarking Progress in Automated Experimental Design and Model Discovery. 2025. arXiv 2501.01540.

Aniketh Garikaparthi, Manasi Patwardhan, and Arman Cohan. ResearchGym: Evaluating Language Model Agents on Real-World AI Research. 2026. arXiv 2602.15112.

Ken Gu et al. BLADE: Benchmarking Language Model Agents for Data-Driven Science. Findings of EMNLP, 2024. ACL Anthology.

Taicheng Guo, Nitesh V. Chawla, Olaf Wiest, and Xiangliang Zhang. AutoLLMResearch: Training Research Agents for Automating LLM Experiment Configuration – Learning from Cheap, Optimizing Expensive. 2026. arXiv 2605.11518.

Hanhua Hong, Yizhi Li, Luu Gia Huy, Jian Yang, Ming Zhou, and Chenghua Lin. Overview of the NLPCC 2026 Shared Task 11: Agent-Based Experiment Reproduction from Scientific Papers. 2026. arXiv 2609.11117.

Qian Huang, Jian Vora, Percy Liang, and Jure Leskovec. MLAgentBench: Evaluating Language Agents on Machine Learning Experimentation. ICML, pp. 20271–20309, 2024. Conference proceedings.

Frank Hutter, Holger Hoos, and Kevin Leyton-Brown. An Efficient Approach for Assessing Hyperparameter Importance. ICML, pp. 754–762, 2014. Conference proceedings.

Peter Jansen, Marc-Alexandre Côté, Tushar Khot, Erin Bransom, Bhavana Dalvi Mishra, Bodhisattwa Prasad Majumder, Oyvind Tafjord, and Peter Clark. DiscoveryWorld: A Virtual Environment for Developing and Evaluating Automated Scientific Discovery Agents. NeurIPS Datasets and Benchmarks, 2024. arXiv 2406.06769.

Nolan Koblischke, Hyunseok Jang, Kristen Menou, and Mohamad Ali-Dib. GravityBench-v1: A Benchmark on Gravitational Physics Discovery for Agents. ICML, 2025. Conference proceedings.

Patrick Tser Jern Kon et al. EXP-Bench: Can AI Conduct AI Research Experiments? ICLR, 2026. Conference proceedings.

Marius Lindauer et al. SMAC3: A Versatile Bayesian Optimization Package for Hyperparameter Optimization. Journal of Machine Learning Research, 23(54):1–9, 2022. Journal paper.

Tennison Liu, Nicolás Astorga, Nabeel Seedat, and Mihaela van der Schaar. Large Language Models to Enhance Bayesian Optimization. ICLR, 2024. arXiv 2402.03921.

Tianyu Liu et al. Benchmarking AI Agents for Addressing Scientific Challenges Across Scales. 2026a. arXiv 2606.12736.

Zejun Liu et al. Can LLM design high-quality experiments? A Comprehensive and Systematic Benchmark on Autonomous Experimental Design. 2026b. arXiv 2608.03501.

Fabian Lukassen, Christoph Weisser, Thomas Kneib, and Alexander Silbersdorff. CAFE: A Compound-AI Factorial Evaluation Framework. 2026. arXiv 2607.10380.

Bodhisattwa Prasad Majumder et al. DiscoveryBench: Towards Data-Driven Discovery with Large Language Models. ICLR, 2025. arXiv 2407.01725.

George B. Moody and Roger G. Mark. The impact of the MIT-BIH Arrhythmia Database. IEEE Engineering in Medicine and Biology, 20(3):45–50, 2001. Dataset version 1.0.0. Dataset record.

Jingjie Ning, Xiaochuan Li, Ji Zeng, Hao Kang, and Chenyan Xiong. Auto Research with Specialist Agents Develops Effective and Non-Trivial Training Recipes. 2026a. arXiv 2605.05724.

Jingjie Ning, Xiaochuan Li, Ji Zeng, Chenyan Xiong, and Guolin Ke. Closed-loop Auto Research for Molecular Property Prediction: Discovering and Certifying Generalizable Improvements. 2026b. arXiv 2606.22731.

Jingjie Ning, Shanshan Zhong, Xiaochuan Li, Ji Zeng, and Chenyan Xiong. One Run Is Not an Idea: The Implementation Lottery in Automated Research. 2026c. arXiv 2607.26587.

Jingjie Ning, Shanshan Zhong, Xiaochuan Li, and Ji Zeng. Scores Alone Do Not Prove Discovery: The Discovery Certification Protocol for Auditing AI Research Agents. 2026d. arXiv 2609.09219.

Ryan O'Donnell. Analysis of Boolean Functions. Cambridge University Press, 2014. Publisher page.

petri-labs. petri-bench: Scoring the Scientific Method of LLM Agents on Procedurally Generated Causal-Discovery Tasks. Technical report, working draft v0.5. Accessed September 15, 2026. Technical report.

Tom Pollard et al. PhysioNet as a global platform for biomedical research. Nature Health, 1:792–795, 2026. Publisher page.

Tom Rainforth, Adam Foster, Desi R. Ivanova, and Freddie Bickford Smith. Modern Bayesian Experimental Design. Statistical Science, 39(1):100–114, 2024. Publisher page.

Arya S. Rao et al. Science sandboxes measure the scientific capability of AI agents. 2026. arXiv 2608.30165.

Carl Edward Rasmussen and Christopher K. I. Williams. Gaussian Processes for Machine Learning. MIT Press, 2006. Online text.

Jerome Sacks, William J. Welch, Toby J. Mitchell, and Henry P. Wynn. Design and Analysis of Computer Experiments. Statistical Science, 4(4):409–423, 1989. Publisher page.

Yujiong Shen et al. SciAgentGym: Benchmarking Multi-Step Scientific Tool-use in LLM Agents. 2026. arXiv 2602.12984.

Jasper Snoek, Hugo Larochelle, and Ryan P. Adams. Practical Bayesian Optimization of Machine Learning Algorithms. NeurIPS 25, 2012. Conference proceedings.

Qiushi Sun et al. ScienceBoard: Evaluating Multimodal Autonomous Agents in Realistic Scientific Workflows. ICLR, 2026. Conference paper.

Nandan Thakur, Nils Reimers, Andreas Rücklé, Abhishek Srivastava, and Iryna Gurevych. BEIR: A Heterogeneous Benchmark for Zero-shot Evaluation of Information Retrieval Models. NeurIPS Datasets and Benchmarks, 2021. Conference proceedings.

Ruoyao Wang, Peter Jansen, Marc-Alexandre Côté, and Prithviraj Ammanabrolu. ScienceWorld: Is your Agent Smarter than a 5th Grader? EMNLP, pp. 11279–11298, 2022. ACL Anthology.

Zhen Wang et al. FIRE-Bench: Evaluating AI Agents on the Rediscovery of Scientific Insights. ICML, 2026. arXiv 2602.02905v2.

Matt L. Wiemann, Lindsay M. Smith, Peter Melchior, Siddharth Mishra-Sharma, Andrew Gordon Wilson, Pavel Izmailov, and Carolina Cuesta-Lázaro. DiscoverPhysics: Benchmarking LLMs for Out-of-the-Box Scientific Thinking. 2026. arXiv 2605.26087.

Yunze Wu et al. InnovatorBench: Evaluating Agents' Ability to Conduct Innovative LLM Research. 2025. arXiv 2510.27598.

Yilun Zhao et al. AbGen: Evaluating Large Language Models in Ablation Study Design and Evaluation for Scientific Research. ACL, 2025. ACL Anthology.

Shanshan Zhong, Yi Lu, Jingjie Ning, Yibing Wan, Lihan Feng, Yuyi Ao, Leonardo F. R. Ribeiro, Markus Dreyer, Sean Ammirati, and Chenyan Xiong. SkillLearnBench: Benchmarking Continual Learning Methods for Agent Skill Generation on Real-World Tasks. COLM, 2026. arXiv 2604.20087.

A Benchmark design and related evaluations

This appendix retains source and option definitions, metric properties, numerical methods, agent prompts, and comparisons needed to interpret the results. Complete configuration, prediction, and trajectory records remain in the accompanying anonymous supplement. Displayed statistics are rounded after computation.

Interactive experimental discovery. ScienceWorld tests grounded scientific reasoning in an interactive text environment (Wang et al., 2022). BoxingGym directly evaluates experimental design and acquired predictive knowledge through expected information gain, prediction errors, and the predictions enabled by an agent's explanation (Gandhi et al., 2025). DiscoveryWorld evaluates complete scientific investigations in virtual worlds, including hypothesis formation, experiments, and conclusions (Jansen et al., 2024). Gravity-Bench budgets observations of gravitational systems and grades numerical answers about concealed physics (Koblischke et al., 2025). Science-Gym couples data collection with equation discovery across physical and epidemiological simulations (Cerrato et al., 2026). SciGym evaluates reconstruction of biological systems (Duan et al., 2025), while DiscoverPhysics scores executable inferred laws and explanations in noncanonical physical worlds (Wiemann et al., 2026). CausalGame evaluates active experimental design and causal explanation in games with selection bias, measurement error, and hidden confounding (Chen et al., 2026). These works establish interactive discovery and prediction as existing benchmark targets. WhatWorkedBench's reference consists of exhaustive native outcomes for documented component interventions, supporting error measurement on every conditional component effect and reuse of identical observations across reconstruction methods.

Understanding and attribution. Science sandboxes explicitly distinguish successful optimization from learning system rules, using regulatory-genomics and protein-fitness settings (Rao et al., 2026). CAFE registers pipeline components as factors, executes factorial designs, and uses mixed-effects models to attribute rated answer quality to components and interactions (Lukassen et al., 2026). The petri-bench technical report evaluates identification of hidden parameter changes and, at its interaction tier, the sign of a controlled two-factor contrast; scoring also checks the supporting experimental procedure (petri-labs, n.d.). WhatWorkedBench grades the entire conditional-effect field implied by a submitted response surface against native metric outcomes. Its cross-comparison contrasts measurement policies under shared estimators and estimators on the same acquired set. Factorial attribution and the distinction between performance and understanding supply foundations for this particular measurement design. DCP grades research-result recovery and calibrated feedback effects under matched controls (Ning et al., 2026d). Our delivered response surface makes intervention knowledge independently gradable.

Research workflows and scientific tools. DeepResearchGym provides a reproducible search environment and evaluates research reports for information-need alignment, retrieval faithfulness, and

quality (Coelho et al., 2026); our fixed experimental environment evaluates quantitative predictions of component interventions. MLAgentBench and MLE-bench evaluate executable machine-learning solutions and model performance (Huang et al., 2024; Chan et al., 2025). BLADE scores analysis decisions against expert analyses (Gu et al., 2024); DiscoveryBench evaluates hypotheses about relationships in supplied datasets through structured facets (Majumder et al., 2025). ScienceAgentBench evaluates executable programs for scientific tasks drawn from publications (Chen et al., 2025). EXP-Bench covers design, implementation, execution, and conclusions for paper-derived experiments (Kon et al., 2026). ResearchGym preserves datasets, evaluators, and baselines while withholding proposed methods (Garikaparthi et al., 2026); InnovatorBench evaluates runnable contributions to LLM research (Wu et al., 2025). Closed-loop molecular Auto Research evaluates feature and model interventions under held-out scoring (Ning et al., 2026b). AstaBench evaluates literature, analysis, coding, and research tasks with reproducible tools and agent baselines (Bragg et al., 2026). RExBench tests expert-specified extensions to existing research code (Edwards et al., 2026). FIRE-Bench evaluates the rediscovery of established findings (Wang et al., 2026). AgentActionBench evaluates reproduction traces using paper-specific rubrics (Hong et al., 2026), and ScienceBoard evaluates scientific workflows using professional software (Sun et al., 2026). SciAgentGym evaluates scientific tool orchestration, and SciAgentArena provides interactive research tasks with stepwise verification (Shen et al., 2026; Liu et al., 2026a). These targets concern successful research actions and outputs. The finite workflow intervention reference here permits exhaustive assessment of what an agent can predict after purchasing only part of the available evidence.

Planning and learned artifacts. AbGen, AblationBench, and SCOPE evaluate proposed ablations or experiment plans using paper-derived references and expert or model judgments (Zhao et al., 2025; Abramovich and Chechik, 2025; Liu et al., 2026b). WhatWorkedBench adds execution-backed measurements and quantitative predictions to the evaluated episode. HExA learns composable skills through active experimentation in Interphyre (Chandra et al., 2026); SkillLearnBench evaluates procedural skills at the levels of skill quality, execution trajectory, and task outcome (Zhong et al., 2026). Here the delivered knowledge artifact is a complete numerical response surface. The Implementation Lottery measures outcome variation across implementations of one research idea (Ning et al., 2026c). Fixed workflow implementations give this benchmark stable references for each documented code-option change.

Design and response-surface foundations. Computer experiments connect budgeted code execution to statistical prediction of computational responses (Sacks et al., 1989). Bayesian experimental design chooses observations to inform a declared target (Rainforth et al., 2024). Deep Adaptive Design learns policies for sequential information acquisition (Foster et al., 2021). Predictive-variance active learning supplies the basis for our grid and linear contrast acquisition criteria (Cohn et al., 1996); the Gaussian-process reference uses standard conditioning and covariance calculations (Rasmussen and Williams, 2006). Functional ANOVA estimates hyperparameter importance and interaction contributions from surrogate models (Hutter et al., 2014). HPOBench provides reproducible optimization objectives, while LLAMBO uses language models for initialization, surrogate modeling, and candidate selection (Eggensperger et al., 2021; Liu et al., 2024). Our exhaustive tables provide observed references for conditional-effect error, allowing different acquisition and inference methods to share one evaluation object. The complete binary-cube representation follows standard Fourier analysis on the Boolean cube (O'Donnell, 2014).

B SOURCE INVENTORY

The catalog contains 30 distinct sources and 36 task conditions. The table links every source identifier to its recorded source location and reports the prepared input and evaluation size. The six entries marked $d = 4/6$ have paired dimensional variants. Their E=F=0 subcubes reproduce the original four-factor outcomes, accounting for 96 repeated configuration records across the two tracks.

Family	Source ID	Prepared input	Evaluation	d
Classification	banknote	943 rows × 4	405 rows	4
	breast_diagnostic	398 rows × 30	171 rows	4
	ionosphere	245 rows × 34	105 rows	4
	spambase	2,947 rows × 57	1,263 rows	4/6
Regression	airfoil	1,052 rows × 5	451 rows	4
	concrete	702 rows × 8	303 rows	4/6
	energy_efficiency	537 rows × 8	231 rows	4
	yacht	215 rows × 6	93 rows	4
Clustering	dry_bean	13,543 rows × 16	7 reference classes	4
	glass	213 rows × 9	6 reference classes	4
	seeds	210 rows × 7	3 reference classes	4
	wine	178 rows × 13	3 reference classes	4/6
Forecasting	co2	1,713 training points	571 next points	4/6
	elnino	549 training points	183 next points	4
	nile	75 training points	25 next points	4
	sunspots	231 training points	78 next points	4
Image restoration	astronaut	256 × 256 pixels	Clean reference	4/6
	coffee	171 × 256 pixels	Clean reference	4
	hubble_deep_field	223 × 256 pixels	Clean reference	4
	rocket	171 × 256 pixels	Clean reference	4
Retrieval	arguana	8,567 documents	64 queries	4
	scifact	5,183 documents	64 queries	4/6
Beat detection	mitdb_100	108,000 at 360 Hz	369 interior events	6
	mitdb_101	108,000 at 360 Hz	340 interior events	6
	mitdb_102	108,000 at 360 Hz	364 interior events	6
	mitdb_103	108,000 at 360 Hz	352 interior events	6
Link prediction	graph_adjnoun	112 nodes, 255 edges	170 cal., 170 test	6
	graph_dolphins	62 nodes, 95 edges	64 cal., 64 test	6
	graph_football	115 nodes, 367 edges	246 cal., 246 test	6
	graph_lesmis	77 nodes, 152 edges	102 cal., 102 test	6

Source terms and attribution. The UCI tabular sources retain CC-BY-4.0 attribution in their manifests. The statsmodels 0.14.6 time-series metadata identify their data as public domain. The scikit-image collection retains source-specific attribution for the NASA Astronaut image, Rachel Michetti's CC0 Coffee image, Hubble Deep Field, and the SpaceX Rocket image. SciFact claims and annotations use CC-BY-4.0, with corpus terms recorded as ODC-By-1.0. ArguAna preserves the original authors' CC-BY-4.0 deposit. MIT-BIH uses Open Data Commons Attribution v1.0 (Moody and Mark, 2001; Pollard et al., 2026).

The graph archive attributes Les Miserables coappearance to D. E. Knuth, *The Stanford GraphBase* (1993); David Copperfield word adjacency to M. E. J. Newman, *Physical Review E* 74, 036104 (2006); college football to M. Girvan and M. E. J. Newman, *PNAS* 99, 7821–7826 (2002); and dolphin associations to D. Lusseau et al., *Behavioral Ecology and Sociobiology* 54, 396–405 (2003). Its source page permits scientific use. Complete source terms, original row counts, duplicate removals, and acquisition metadata remain with each source manifest.

Photographs share the scikit-image collection, time series share the statsmodels distribution, ECG records share MIT-BIH, and graph instances share an archive. Source-level reporting retains these relationships and merges paired variants when counting distinct sources.

C Data preparation and evaluation boundaries

C.1 Tabular classification, regression, and clustering

The UCI metadata define feature roles, index columns, and target columns. Acquisition checks the dataset identifier and feature count against these metadata. Regression uses the designated numerical target. Energy Efficiency uses heating load Y1, with the secondary target excluded from the features.

Classification and clustering map sorted original class labels to integer identifiers. All retained feature and target values are finite.

Preparation removes exact duplicate feature–label rows while preserving the order of first occurrence. Supervised datasets then group rows by identical feature vectors. A single `GroupShuffleSplit` with evaluation fraction 0.3 and seed 20260907 assigns complete groups to training or evaluation. Both parts of every classification split contain the same class set. The split is fixed across masks. Feature transforms, feature selection, PCA, and predictive models fit on training data and transform the evaluation features afterward.

Clustering operates on all deduplicated feature rows. The known number of classes fixes k. K-means fits the feature representation for each mask, and the original class labels enter the external NMI calculation. The evaluation therefore measures agreement between the resulting partition and the archived class partition on the fixed data.

C.2 Chronological forecasting

The time-series files come from statsmodels version 0.14.6. El Niño year rows are expanded in calendar-month order. Other series preserve their source time order. A missing value receives the latest preceding finite value. CO2 has 59 such replacements, and the other three series have zero. The training cut is $\lfloor 0.75N \rfloor$, and the suffix supplies the evaluation points.

All configurations start their training examples at index 12 so the one-lag and 12-lag designs use the same fitting times. The predictor fits once on the training prefix. Evaluation at time t uses the realized observations preceding t, giving a sequence of one-step predictions with fixed fitted parameters. The six-factor first-difference option applies after the optional logarithm and restores each prediction using the preceding realized level. This contract defines the temporal information available to every mask.

C.3 Image preparation and restoration

Image bytes are checked against the scikit-image 0.26.0 registry. Pillow converts the source to grayscale, uses a Lanczos thumbnail with maximum width and height 256, and scales intensities by 255. The resulting array supplies the clean reference. A NumPy generator with seed 20260907 adds independent Gaussian noise with standard deviation 0.1, followed by clipping to $[0, 1]$. Each source uses the same prepared noisy array across all masks. Native filters operate on that array, and the clean array enters only the external pixel-RMSE calculation.

C.4 Retrieval corpora and query cohorts

The retrieval sources use BEIR corpus exports (Thakur et al., 2021). SciFact uses 5,183 corpus documents and the hash-first 64 original training queries. ArguAna uses 8,567 corpus documents and the first 64 prepared G queries from its original training partition. Original relevance annotations supply the target. Corpus documents are sorted by document identifier before vectorizer fitting. Query vectors use the corpus-fitted vocabulary and weighting. Stable descending score order determines the top ten documents.

ArguAna removes every document whose normalized text matches the query text, under every mask. The recorded split audit checks query text, counter-text, reversed pairs, and debate-group relationships. The prepared query cohorts and the source terms are preserved in the source manifests. Retrieval utility averages the same 64 query-level NDCG values for every configuration.

C.5 Archived signal records

MIT-BIH records 100, 101, 102, and 103 contribute samples $[0, 108000)$ from channel zero at 360 Hz. The first channel's physical units are millivolts. WFDB reads the waveform and original event annotations. The QRS label-code set is $\{1, 2, 3, 4, 5, 6, 7, 8, 9, 10, 11, 12, 13, 25, 30, 31, 34, 35, 38, 41\}$, following the source labels.

Native prediction receives the waveform and sample rate. Scoring restricts predicted and reference events to the interior $[1, 299)$-second interval. The source inventory reports the interior event counts

used for scoring. The filters use offline forward–backward filtering. Consequently, this task evaluates event localization within a fixed archived segment. Event matching uses a 100-ms tolerance, with 50-ms and 150-ms checks retained for sensitivity.

C.6 Graph construction and pair partitions

The source graphs are converted to simple, undirected, unweighted graphs. Self-loops are removed and node identifiers are mapped to consecutive integers. A source-specific fixed seed shuffles the original edges. Calibration and test each receive $\mathrm{round}(0.2|E|)$ positive edges. The remaining edges form the observed graph, giving approximately 60/20/20 proportions. The shuffled sequence assigns observed edges first, then calibration positives, then test positives. Partition sizes and source-specific seeds accompany the prepared arrays.

Calibration and test negatives are disjoint balanced samples from the original graph's nonedges. Every feature for both sets is computed on the shared observed graph. Calibration labels fit logistic regression. Test labels supply the external ROC AUC. This creates a reproducible finite link-prediction problem with separate observed, calibration-positive, and test-positive edges.

D Workflow options and fixed numerical settings

Mask bits run left to right as A, B, C, D, E, F. The four-factor track uses A–D. The paired track adds E and F with the original options and order preserved. Every binary mask is legal. The tables specify both settings for each option, followed by operation order and numerical details. The public task files contain the corresponding executable operation definitions.

D.1 Classification

Bit	Setting 0	Setting 1
A	Original features	$\mathrm{sign}(x)\log(1+\lvert x\rvert)$
B	Original feature scale	Training-fitted standard scaling
C	Uniform class weights	Balanced class weights
D	Logistic regression $C = 1$	Logistic regression $C = 0.05$
E	All input features	Training-fitted ANOVA selection at the 50th percentile
F	Input representation	PCA retaining 95% variance after optional selection

Logistic regression uses the LBFGS solver, 3,000 maximum iterations, and random state 17. Standard scaling precedes selection and PCA. PCA uses the full SVD. Class balancing follows the training class frequencies.

D.2 Regression

Bit	Setting 0	Setting 1
A	Original target	Training-target `log1p` with `expm1` inverse
B	Original feature scale	Training-fitted feature scaling
C	Original features	Degree-two polynomial features without a bias column
D	Ridge $\alpha = 1$	Ridge $\alpha = 10$
E	Full degree-two polynomial terms	Interaction-only polynomial terms when C is enabled
F	Standard scaling when B is enabled	Robust scaling when B is enabled

Scaling precedes polynomial construction. Ridge uses the SVD solver. The target transform wraps the complete regressor. E is inactive at C=0, and F is inactive at B=0.

D.3 CLUSTERING

Bit	Setting 0	Setting 1
A	Original features	Signed logarithmic feature transform
B	Original feature scale	Feature-only standard scaling
C	All input features	PCA retaining 95% variance
D	One k-means initialization	Ten k-means initializations
E	Unwhitened PCA coordinates	Whitened coordinates when C is enabled
F	K-means++ initialization	Random initialization

K-means uses Lloyd's algorithm, a maximum of 300 iterations, and random state 17. The known class count determines k. PCA uses the full SVD. E is inactive at C=0.

D.4 FORECASTING

Bit	Setting 0	Setting 1
A	Lag features	Lag features and a linear time trend t/cut
B	Lag 1	Lags 1 through 12
C	Original series levels	`log1p` levels with `expm1` inverse
D	Ridge $\alpha = 1$	Ridge $\alpha = 10$
E	Training-fitted standard scaling	Training-fitted robust scaling
F	Model series levels	Model first differences and restore the previous level

Ridge uses the SVD solver. Optional differencing follows the series transform. The first difference at index zero is set to zero, and fitting starts at index 12 for every mask. Forecast inversion restores differenced levels before the optional exponential inverse.

D.5 IMAGE RESTORATION

Bit	Setting 0	Setting 1
A	Pass the image onward	Median filter with a 3×3 window
B	Pass the image onward	Gaussian filter with $\sigma = 0.8$
C	Pass the image onward	Wiener filter with a 5×5 neighborhood
D	Pass the image onward	Unsharp mask with Gaussian $\sigma = 1$, amount 0.5
E	Gaussian $\sigma = 0.8$ when B is enabled	Gaussian $\sigma = 1.6$ when B is enabled
F	Median window 3×3 when A is enabled	Median window 5×5 when A is enabled

Filters execute in A, B, C, D order and the final image is clipped to $[0, 1]$. Median and Gaussian filters use reflected boundaries. Wiener noise power is estimated by the library from the current image. E is inactive at B=0 and F is inactive at A=0.

D.6 RETRIEVAL

Bit	Setting 0	Setting 1
A	Unigrams	Unigrams and bigrams
B	Retain stopwords	Remove the scikit-learn English stopword set
C	Raw term frequency	Sublinear term frequency
D	Unit term weights	Inverse-document-frequency weighting
E	Frequency counts	Binary term counts
F	L2 vector normalization	Unnormalized document and query vectors

TF–IDF vectors use float64. The vectorizer fits on corpus text and transforms queries. Dot products supply ranking scores. Binary counts make the sublinear transform inactive. Document sorting and stable ranking fix score ties.

D.7 BEAT DETECTION

Bit	Setting 0	Setting 1
A	Median-centered waveform	Additional second-order 0.5-Hz high-pass filter
B	Current waveform	Additional second-order 35-Hz low-pass filter
C	Absolute-amplitude envelope	Squared first-difference envelope
D	Current envelope	120-ms moving integration
E	Mean plus one standard deviation	Median plus three scaled MAD units
F	200-ms minimum peak distance	300-ms minimum peak distance

The MAD scale factor is 1.4826. Butterworth filters use second-order sections and forward–backward filtering. Integration uses nearest-edge extension. Each candidate aligns to the largest absolute filtered amplitude within 75 ms. Duplicate samples merge before scoring.

D.8 LINK PREDICTION

Bit	Setting 0	Setting 1
A	Feature absent	Common-neighbor count
B	Feature absent	Jaccard coefficient
C	Feature absent	Adamic–Adar index
D	Feature absent	Resource-allocation index
E	Feature absent	Preferential-attachment score
F	Original feature scales	Calibration-fitted standard scaling

A mask with all five feature bits zero supplies a zero feature column and fits an intercept-only model. Logistic regression uses $C = 1$, LBFGS, 2,000 maximum iterations, and random state 20260907. The positive-class probability supplies the ranking score for ROC AUC.

E RESPONSE SCALES AND CONDITIONAL STRUCTURE

The table summarizes response widths $\max_z u_t(z) - \min_z u_t(z)$ and effect magnitudes by workflow family. Each interval spans task conditions within that family. A_t is the mean absolute conditional effect used to normalize recovery. The released `results/conditional_effects.csv` preserves every source, mask pair, and native outcome; the source inventory links each condition to its dataset or record.

Workflow	Conditions	Response range ($\max - \min$)	Mean effect A_t
Regression	5	0.0402–0.3847	0.0096–0.1018
Retrieval	3	0.3094–0.6394	0.0755–0.0992
Image restoration	5	0.1928–0.3306	0.0401–0.0678
Classification	5	0.0364–0.2799	0.0081–0.0391
Forecasting	5	0.0109–0.1594	0.0026–0.0384
Clustering	5	0.1733–0.8203	0.0433–0.1362
Beat detection	4	0.4464–0.6268	0.0538–0.1299
Link prediction	4	0.2470–0.4035	0.0199–0.0366

F METRIC DEFINITIONS AND ARTIFACT GRADING

F.1 COVERAGE OF JOINT INTERVENTIONS

Let $x = z_0, z_1, \ldots, z_k = y$ be a path that switches each differing bit once. Then

$$\sum_{j=1}^{k} [u(z_j) - u(z_{j-1})] = u(y) - u(x). \tag{3}$$

Each summand is a signed conditional component effect. Exact effects therefore determine every joint intervention and, with one anchor, every utility value. Predicted effects derived from a complete table satisfy the same identity. If every edge error is bounded by ϵ, the triangle inequality bounds the k-switch intervention error by $k\epsilon$. This statement applies to maximum edge error; mean edge MAE describes average reconstruction quality. Higher-order interactions remain represented through the background dependence of conditional effects. Mean pair interactions provide a readable summary of that structure and may average effects with different signs.

F.2 Configuration choice and effect recovery

Both two-bit tables below preserve the free anchors and select 10 as their unique optimum for $0 < \delta < 1$.

Configuration	00	10	01	11
True utility	0	1	0	0
Predicted utility	0	1	$1-\delta$	0

The mean absolute true edge effect is $A = 1/2$ and edge MAE is $E = (1-\delta)/2$, giving $R = \delta$. Thus exact choice can coexist with arbitrarily weak effect recovery. Additional inactive bits embed the same construction in four- and six-factor spaces. This example explains the distinct evaluation targets; the main results measure their relationship on native workflows.

F.3 Native metrics and utility transformations

Balanced accuracy is the arithmetic mean of class recalls. NMI uses $2\,\mathrm{MI}(Y,C)/[H(Y)+H(C)]$, with contingency counts defining the entropies and mutual information. Regression and forecasting use the arithmetic mean absolute residual. Image restoration uses the square root of mean squared pixel residual. Retrieval uses

$$\mathrm{NDCG@10}(q) = \frac{\sum_{k=1}^{10} r_q(\pi_k)/\log_2(k+1)}{\sum_{k=1}^{10} r_{q,(k)}/\log_2(k+1)}, \tag{4}$$

where r_q is the original binary relevance and $r_{q,(k)}$ is its sorted ideal gain. Utility averages this quantity over the fixed query cohort.

Event F1 is $2M/(P+T)$, where P and T are the numbers of interior predicted and reference events, and M is the maximum number of one-to-one pairs within the matching tolerance. The sorted native matcher is checked by a separately implemented maximum bipartite matcher. ROC AUC averages pairwise ranking credit over positive and negative examples, awarding one for a higher positive score and one-half for a tie.

Balanced accuracy, NMI, NDCG, event F1, and ROC AUC directly supply utility. For native cost c in regression, forecasting, or restoration,

$$u = \frac{1}{1+c/s}, \qquad c = s\left(\frac{1}{u}-1\right). \tag{5}$$

Regression uses the interquartile range of training targets for s. Forecasting uses the interquartile range of the training series. Restoration uses $s = 0.1$. The fixed training statistics define the scale for every mask.

F.4 Effect, interaction, and grid errors

The main text defines conditional-effect MAE E_t and recovery R_t. Pair interaction J_{ij} averages the second difference over all 2^{d-2} backgrounds, and pair MAE is

$$I_t = \binom{d}{2}^{-1} \sum_{i<j} |\widehat{J}_{ij} - J_{ij}|. \tag{6}$$

Grid MAE is $G_t = 2^{-d}\sum_z |\hat{u}(z) - u(z)|$. The anonymous supplement records E_t, I_t, G_t, and grid error on unobserved cells for every scored artifact.

Selection chooses the largest predicted utility, then fewer enabled bits, then the lexically smaller mask. Regret compares that mask's true utility with the exhaustive optimum. Exact choice allows regret at most 10^{-12}. A supplemental near-optimal flag uses regret at most 0.02 utility, accompanied by an indicator for tasks whose entire response range is below 0.02.

F.5 Artifact validation and the strict diagnostic

A complete artifact contains exactly one finite numerical utility in $[0, 1]$ for each legal mask. Duplicate JSON keys, Boolean values in numerical cells, nonfinite values, missing cells, and extra masks fail validation. The grader replaces measured cells with their authoritative observed values before computing effects and selection. Submission closes the episode.

Strict reconstruction is

$$S_t(\tau) = \mathbf{1}\left[\max_{i,z:z_i=0} |\widehat{\Delta}_i(z) - \Delta_i(z)| \le \max\{10^{-12}, \tau(\max u_t - \min u_t)\}\right]. \tag{7}$$

The development endpoint uses $\tau = 0.1$. Missing delivery receives $R_t = 0$, $S_t = 0$, and zero exact-choice credit. Its raw numerical errors remain undefined. Shared estimators can still use the observations acquired before that failure.

F.6 Measured effects and remaining reconstruction

The complete-effect score includes knowledge supplied by direct measurement and by predictions at unmeasured configurations. Let K contain edges whose endpoints are both observed, let U contain the remaining edges, and let $c = |K|/(|K| + |U|)$. Restoring authoritative observations makes the error on K zero. Hence

$$E_t = (1 - c)E_{U,t}, \qquad E_{U,t} = \frac{1}{|U|}\sum_{e\in U} |\widehat{\Delta}_e - \Delta_e|, \qquad Q_{U,t} = E_{U,t}/A_t. \tag{8}$$

Lower Q_U indicates smaller error on effects involving unmeasured endpoints. The task-wide A_t fixes its scale across observation policies. Each policy determines the remaining edge set.

A simple calibration completes every unmeasured utility with the mean of that episode's observed utilities. This baseline and the agent artifact receive exactly the same observations and observed-cell restoration. The retrospective analysis covers all 94 valid core artifacts; the table presents Flash results separately for the original (O) and additional (A) cohorts. Repeated executions are averaged within source and cohort. N counts represented sources. Columns labelled mean use the completion baseline; agent columns use delivered tables.

Setting	B	Valid	N	Known edges	R_{mean}	R_{agent}	$Q_{U,\text{mean}}$	$Q_{U,\text{agent}}$
O, 4 factors	4	6	6	10.4%	0.056	0.178	1.093	0.921
O, 4 factors	8	12	6	32.6%	0.287	0.632	1.054	0.542
O, 6 factors, full	20	6	6	6.8%	0.012	0.268	1.156	0.824
O, 6 factors, opaque	20	6	6	14.9%	0.011	0.257	1.183	0.899
A, 4 factors	4	12	6	9.9%	0.084	0.375	1.075	0.710
A, 4 factors	8	6	6	32.3%	0.213	0.621	1.156	0.567
A, 6 factors, full	20	10	6	8.6%	0.014	0.211	1.200	0.882
A, 6 factors, opaque	20	9	6	8.8%	0.028	0.283	1.172	0.790

For the original Flash cohort at $B = 8$, 32.6% of effects have two measured endpoints, leaving 67.4% dependent on reconstruction. Mean completion gives recovery 0.287 and $Q_U = 1.054$, while the delivered tables give 0.632 and 0.542. Shared GP gives recovery 0.698 and $Q_U = 0.444$ on the same observations. The original six-factor views also improve over mean completion, with 85.1%–93.2% of effects involving an unmeasured endpoint. Per-episode coverage and errors remain in the anonymous supplement. This analysis adds a calibration view of the saved artifacts and preserves the original 4,206 numerical-control records and primary scoring definition.

G NUMERICAL ESTIMATORS AND MEASUREMENT POLICIES

G.1 MAIN-EFFECT AND PAIR-EFFECT RIDGE

For mask z, the feature vector contains an intercept and products of centered bits $x_i = 2z_i - 1$. Degree one includes x_i; degree two adds $x_i x_j$ for all $i < j$. For measured set O, ridge solves

$$\min_{\beta_0,\beta} \sum_{z\in O} [u(z) - \beta_0 - \phi(z)^\top \beta]^2 + \alpha\|\beta\|_2^2. \tag{9}$$

The intercept is unpenalized. Each candidate α in $\{10^{-5}, 10^{-3}, 0.1, 1, 10\}$ is evaluated by leaving out one measured observation at a time. Mean squared error selects the regularizer. Loss ties at 14 decimal places prefer larger α. The final table is clipped to $[0, 1]$ and measured cells are restored.

The sequential design policy uses the same factorial feature vector, including the intercept, and selects the remaining mask with maximum

$$\phi_{\text{all}}(z)^\top \left(X_O^\top X_O + \text{diag}(10^{-8}, 0.01, \ldots, 0.01)\right)^{-1} \phi_{\text{all}}(z). \tag{10}$$

Each chosen row enters the design matrix before the next selection. Utility values enter ridge fitting; the design depends on feature geometry and the already selected masks. Acquisition ties at ten decimal places prefer lexical mask order. D1 denotes degree-one design and fitting, and D2 denotes degree-two design and fitting. Rand2 samples a uniformly shuffled legal-mask sequence without replacement and fits degree-two ridge. Each random setting has 20 recorded seed indices, numbered 0 through 19, added to seed base 20260907.

G.2 GAUSSIAN-PROCESS CONTROLS

The all-order kernel is $k(z, z') = \exp[-h(z, z')/\ell]$, where h is Hamming distance. Ordinary kriging estimates a constant mean from measured values (Rasmussen and Williams, 2006). For $C = K_O + \eta I$, let

$$q = C^{-1}\mathbf{1}, \quad c = \mathbf{1}^\top q, \quad P = C^{-1} - qq^\top/c. \tag{11}$$

The leave-one-out residual vector has entries $(Py)_i/P_{ii}$. Its mean square selects $\ell \in \{0.25, 0.5, 1, 2, 4, 8\}$ and $\eta \in \{10^{-6}, 10^{-3}, 0.03, 0.3\}$. Loss ties at 14 decimal places prefer larger length scale, then larger nugget. The nugget regularizes the fit to deterministic utilities. Predictive means are clipped and observations restored.

Let Σ be the ordinary-kriging covariance on the full grid and D the matrix taking all conditional component differences. The two acquisition objectives for candidate j apply predictive-variance reduction (Cohn et al., 1996) to the grid and its linear contrasts, respectively, giving

$$a_G(j) = \frac{\|\Sigma_{:,j}\|_2^2}{\max(\Sigma_{jj} + \eta, 10^{-12})}, \qquad a_E(j) = \frac{\|D\Sigma_{:,j}\|_2^2}{\max(\Sigma_{jj} + \eta, 10^{-12})}. \tag{12}$$

GP-G maximizes a_G and GP-E maximizes a_E. Parameters are refitted after each new observation. Acquisition ties at 12 decimal places prefer lexical mask order. The grid and effect objectives share the same estimator.

G.3 PROGRAM-EQUIVALENCE CONTROLS

The six-factor control maps masks to representatives using the visible guards in Section D. In regression, E resets to zero when C is zero, and F resets to zero when B is zero. In clustering, E resets to zero when C is zero. In restoration, E resets to zero when B is zero, and F resets to zero when A is zero. In retrieval, C resets to zero when E is one. Classification and forecasting retain all masks as separate representatives.

These rules yield 64, 36, 48, 64, 36, and 48 classes in classification, regression, clustering, forecasting, restoration, and retrieval, respectively. Every asserted alias matches the native prediction hash and utility of its representative. CD1 and CD2 apply the corresponding ridge design and fit to representatives. CGP-E computes its kernel on representative masks and uses effect-variance acquisition. Purchased observations and inferred aliases are recorded separately. Once every class is measured, the policy stops purchasing and maps measured values to the complete grid. Thus actual credits b can be below the allowed budget B.

G.4 SHARED ESTIMATORS AND AGGREGATION

Shared fitting passes the exact observed set from an episode to D1, D2, or the GP. It then evaluates the resulting complete table against the same reference. The GP uses the fitting rule above with the observed set fixed. Its own acquisition policy remains inactive during a shared fit. Episodes with missing delivery retain their acquired observations for this analysis.

For random designs, metrics average over seeds within a source. Core repeat studies average trials within a source. Family-macro scores then average sources within each family and weight the participating families equally. Four-factor controls use all 22 source instances, the paired six-factor controls use the six paired sources, and the added track uses four sources within each of its two families. Agent–control comparisons select the same six source instances. Reported counts retain their episode or source denominator explicitly. The prospective typed cohort averages sources equally and conditions R_{del} on valid delivery, with source-level resampling for its intervals.

H CORE AGENT INTERFACE AND EXECUTION ENVIRONMENT

The core four-factor and paired six-factor studies expose four tools. `current_evidence()` returns the public task, observations, remaining credits, calculation allowance, elapsed time, remaining time, and episode status. `observe_many(masks)` purchases a batch of legal configurations. `calculate_python(code)` runs numerical Python with the current public task and observations. The final submission tool registers a prediction table or a public estimator selection. Appendix K.4 specifies the independent six-factor typed study.

The four-factor observation tool accepts 1–14 masks per call, and the paired six-factor tool accepts 1–62. Repeated masks consume zero additional credits. A batch is checked in full before charging or inserting observations. A valid batch charges one credit per distinct newly measured mask. At B purchased measurements, the total observed set has at most $B + 2$ cells. Native configuration outcomes are cached from the reference construction.

Four-factor receipts include utility, native metric name, and native metric value. Both views of the six-factor information study use utility-only receipts. The full view contains workflow code, factor semantics, source information, and input summaries. The opaque view contains a generic workflow identifier, dimensions, factor order, legal masks, and the scalar utility contract. The opaque view's identifiers and receipts preserve that information condition.

Every numerical call starts a fresh Python process with the current observations and task. NumPy, SciPy, scikit-learn, and `wwb_helpers` are available. The process receives a 30-second CPU ceiling, 45-second wall ceiling, 2-billion-byte address-space ceiling, and 2-million-byte file-size ceiling. CPU affinity uses at most two available cores. The surrounding namespace mounts public task data, helpers, and numerical dependencies. Network access and bundled scikit-learn dataset labels are blocked. Printed outputs return to the agent for subsequent reasoning. A maximum of 20 calculation calls applies to each episode.

The evaluated models are the recorded identifiers `deepseek-v4-flash` and `deepseek-v4-pro`. Runs enable reasoning, request high effort, and set an output-token cap of 32,768 with a 1,800-second outer session deadline. The broker checks time before further investigation calls and accepts a final submission while the outer session remains active. Tool receipts expose the remaining investigation time. The prompt advises submission with 120 seconds remaining. The public helper names are `ridge_main` and `ridge_pair`, both recorded explicitly in submission metadata.

I RECORDED AGENT PROMPTS AND TASK PAYLOADS

The source bundle includes the complete frozen strings in `prompts/four_system.txt`, `prompts/four_prompt.txt`, `prompts/six_system.txt`, and `prompts/six_prompt.txt`. The anonymous supplement preserves the same templates in `benchmark/prompts/`. Episode construction substitutes the measurement budget, two anchor observations, and public task into the templates.

The instructions prioritize conditional-effect accuracy and require predictions for all 16 or 64 configurations. They state the session and calculation limits, describe the numerical helpers, and permit either a complete prediction table or explicit helper selection. Submission is recommended with 120 seconds remaining. Four-factor repetitions share the original prompt strings. Both six-factor information views share the templates; their public task payloads specify the information condition.

The structure diagnostic adds a first-call request for a JSON list of inactive-option rules. Both arms receive this request; one additionally receives verified rules in its task payload (Appendix K.3). Its exact instruction and supplied payloads are included with the diagnostic records. The task pack contains full workflow code and each agent's received payload.

J STUDY DESIGN AND EXECUTION ACCOUNTING

Construction and analysis order. The 22-source four-factor inventory is specified before execution of its added configurations. Paired construction extends the six initial agent-evaluation sources, Spambase, Concrete, Wine, CO_2, Astronaut, and SciFact, with E and F and requires agreement with their original subcubes. The signal and graph extension lists eight sources and fixes its numerical methods and budgets before native outcomes. Every listed source appears in the final catalog. Acceptance uses native validity, cold replay, independent metric agreement, and evaluation-boundary checks.

Plans for ridge/design, GP, and code-equivalence controls record source selection, budgets, and code identities. The core agent cohort, paired information study, original-cohort second $B = 8$ Flash trial, and 66-episode repeat retain their prompts, tools, deadlines, model identifiers, and execution dates. The six-factor information study specifies shared-GP evaluation in its plan; the core-cohort shared-GP fit is retrospective on saved observations. The repeat comprises 42 four-factor and 24 six-factor information executions. Tolerance, native-unit, and sign analyses use saved references and predictions.

Budgets and records. Four-factor controls use $B \in \{0, 4, 8, 14\}$; paired six-factor controls use $B \in \{0, 4, 8, 14, 20, 32, 62\}$; the eight added sources use $B \in \{0, 8, 20, 32, 62\}$. The 4,206 records comprise 1,936 four-factor ridge/design runs, 924 paired ridge/design runs, 84 code-equivalence ridge runs, 302 GP runs, and 960 added-source runs. Random designs use 20 seed indices. Full-observation endpoints purchase every remaining mask or program-equivalence class.

Agent study	d	B	Episodes	Delivered
Flash and Pro original cohort	4	4, 8	24	20
Flash full/opaque information	6	20	12	12
Flash original, second $B = 8$ trial	4	8	6	6
Additional Flash and Pro	4	4, 8	42	37
Additional Flash information	6	20	24	19
Structure diagnostic	6	20	8	8
Typed estimator-menu study	6	20	8	8
Fixed-observation inference	6	0	4	4
Typed source cohort	4	8	24	23
Added beat/graph workflows	6	32	8	6
All studies			**160**	**143**

The first five rows comprise 108 core episodes. The added-family row includes six delivered tables and two source attempts without final artifacts; the delivered-table analysis in Appendix L.6 uses all six. Core accounting retains every attempted provider request and excludes five zero-request administrative records. Four original-cohort Pro episodes end at their 1,800-second deadlines after 4, 12, 23, and 14 HTTP 429 responses; the original four-factor cohort records 75 HTTP 429 responses in total. Five additional-cohort Pro episodes also end without final artifacts, with zero HTTP 429 responses across that cohort. The typed-source Pro Astronaut episode runs in the four-session final batch, purchases all eight measurements, and reaches its 1,800-second deadline without a final table. The original, information, and repeat studies record 748, 304, and 155 terminal requests, respectively. Provider identifiers, response status, usage, timing, and observation events remain in the anonymous supplement.

K EPISODE RESULTS AND PAIRED COMPARISONS

Table 6 separates delivery, all-attempt recovery, recovery conditional on delivery, and shared-GP recovery on acquired observations.

Table 6: Four-factor agent evaluation on six matched sources. Delivery is complete artifacts over attempts. R_{all} averages all attempts with zero for missing artifacts; R_{del} averages delivered artifacts; R_{GP} fits a common GP to observations from all attempts. Exact and strict count episodes.

Model	Cohort	B	Delivery	R_{all}	R_{del}	R_{GP}	Exact	Strict
Flash	Original	4	6/6	0.178	0.178	0.226	2	0
Flash	Original	8	12/12	0.632	0.632	0.698	5	1
Pro	Original	4	4/6	0.043	0.064	0.346	2	0
Pro	Original	8	4/6	0.366	0.549	0.692	3	0
Flash	Additional	4	12/12	0.375	0.375	0.338	5	0
Flash	Additional	8	6/6	0.621	0.621	0.720	2	0
Pro	Additional	4	10/12	0.308	0.370	0.315	2	0
Pro	Additional	8	9/12	0.503	0.671	0.667	6	1

The compact calibration table retains repetition variability and a mean-fill reference. Within-source SD averages the sample SD of all-attempt recovery across repetitions within each source; a dash marks one execution per source. Mean-fill recovery preserves purchased scores and fills other configurations with their observed mean. Its denominator n_{fill} counts delivered tables. The released `results/agent_index.json` retains all 108 core episode records, predictions, measurements, helper choices, and execution metadata.

Model	Cohort	B	Within-source SD	Mean-fill R	n_{fill}
Flash	Original	4	–	0.056	6
Flash	Original	8	0.073	0.287	12
Pro	Original	4	–	0.045	4
Pro	Original	8	–	0.326	4
Flash	Additional	4	0.105	0.084	12
Flash	Additional	8	–	0.213	6
Pro	Additional	4	0.130	0.115	10
Pro	Additional	8	0.080	0.273	9

K.1 INFORMATION SUPPLIED TO THE AGENT

Full and opaque conditions share sources, reference tables, budgets, tools, helpers, utility-only receipts, and deadlines. Full information adds code, option semantics, source information, and input summaries jointly. Each source has one attempted pair in the original cohort and two in the additional cohort. The table reports R_{all} and shared-GP recovery; Δ is full minus opaque.

Cohort	Source	Valid pairs	R_{all}			Shared GP R		
			Full	Opaque	Δ	Full	Opaque	Δ
O	astronaut	1/1	0.294	0.255	+0.039	0.379	0.137	+0.242
O	co2	1/1	0.244	0.049	+0.196	0.263	0.131	+0.133
O	concrete	1/1	0.298	0.642	-0.343	0.796	0.847	-0.051
O	scifact	1/1	0.522	0.407	+0.115	0.598	0.468	+0.130
O	spambase	1/1	0.000	0.000	+0.000	0.000	0.389	-0.389
O	wine	1/1	0.247	0.191	+0.056	0.205	0.414	-0.209
A	astronaut	1/2	0.275	0.000	+0.275	0.217	0.112	+0.105
A	co2	1/2	0.129	0.102	+0.027	0.262	0.161	+0.101
A	concrete	2/2	0.505	0.754	-0.249	0.771	0.843	-0.072
A	scifact	1/2	0.153	0.357	-0.204	0.300	0.496	-0.195
A	spambase	2/2	0.042	0.000	+0.042	0.039	0.203	-0.164
A	wine	1/2	0.006	0.193	-0.187	0.002	0.160	-0.158

Cohorts O and A denote original and additional executions. Valid pairs count pairs with two delivered artifacts over all attempted pairs. Means retain all attempts, including $R_{\text{all}} = 0$ after a missing submission. The original mean R_{all} difference is 0.0103 and its shared-GP difference is -0.0242. Additional-cohort differences are -0.0491 for R_{all} and -0.0638 for shared GP. The eight additional pairs with two delivered artifacts cover all six sources; their source-macro differences are -0.1198 and -0.0914, respectively. These conditional summaries describe the paired deliveries, while the main comparison retains every attempted pair.

K.2 Repeated high-budget agent runs

Both original Flash $B = 8$ trials and the additional execution are retained for each source. The table keeps their cohorts separate. Parentheses give the sample standard deviation where repetitions are available; a dash denotes a single execution. The final column reports matched D2 recovery.

Source	Flash, original		Flash, additional		Designed D2
	R_{all} (SD)	Shared GP	R_{all} (SD)	Shared GP	R
astronaut	0.356 (0.144)	0.645	0.270 (—)	0.523	0.634
co2	0.365 (0.026)	0.505	0.569 (—)	0.667	0.400
concrete	0.853 (0.011)	0.877	0.842 (—)	0.913	0.888
scifact	0.803 (0.096)	0.799	0.762 (—)	0.761	0.799
spambase	0.637 (0.066)	0.667	0.684 (—)	0.683	0.508
wine	0.778 (0.095)	0.691	0.599 (—)	0.775	0.533

Across the 12 original episodes, five select an exact optimum and one passes strict reconstruction. Original mean recovery is 0.6321 and shared GP recovery is 0.6976. The six additional episodes have mean recovery 0.6211 and shared GP recovery 0.7205, with two exact choices and zero strict reconstructions. The anonymous supplement indexes every measurement batch and prediction.

K.3 Rule recognition and application

This rule-reporting diagnostic uses all four six-factor workflows with nontrivial code equivalences. Each source receives one full-code and one code-plus-rules Flash episode at $B = 20$, with arm order alternated across sources. Both arms use the full task and the same first-call instruction to report inactive-option rules before buying measurements. The report counts toward the 20 calculation calls and receives no correctness feedback. The rules arm additionally receives six registered guard relations across the four sources. Independent checks confirm identical native predictions for all 96 registered equivalent endpoint pairs. Models, tools, anchors, and session limits match the information study. These eight episodes were run on September 22, 2026 (UTC), as a separate cohort with an elicited reporting task.

The table separates observable rule reporting, acquisition, and prediction. Rules counts correctly reported registered relations. Redundant counts purchases within an equivalence class already represented by an anchor or paid measurement. Equiv. error is the mean absolute predicted-utility difference across the registered equivalent pairs, divided by the source's utility range. Recovery retains all attempted episodes. The final column is an offline class-consistent control applied to each frozen submission. A class containing a measured mask receives that observation; other classes receive the mean of their submitted predictions. The projection preserves every acquired observation and uses no new measurements. All eight episodes deliver valid artifacts.

Source	Information	Rules	Redundant	Equiv. error	Recovery	Class R
concrete	Code	2/2	0/20	4.88%	0.680	0.823
concrete	Code + rules	2/2	0/20	10.21%	0.646	0.748
wine	Code	1/1	0/20	16.97%	0.000	0.000
wine	Code + rules	1/1	0/20	15.54%	0.213	0.290
astronaut	Code	2/2	2/20	16.77%	0.000	0.415
astronaut	Code + rules	2/2	0/20	12.14%	0.334	0.745
scifact	Code	1/1	0/20	8.89%	0.308	0.485
scifact	Code + rules	1/1	0/20	1.39%	0.524	0.549

Both arms correctly report all six registered rules. The rules-supplied arm has higher recovery on three sources and lower recovery on concrete; arm means are 0.247 and 0.429. Shared GP reaches 0.382 and 0.471. The code arm spends 2/80 credits on equivalent repeats and the rules arm spends none. All eight final artifacts use public ridge helpers and violate equivalences, with mean equivalence errors of 11.88% and 9.82% of source utility range. The class-consistent control scores mean recovery 0.507 versus 0.338 for the delivered tables at fixed observations. It has lower raw effect error in all eight episodes and higher recovery in seven; the strict score remains zero. These source pairs separate reported rules from delivered ridge-helper predictions and quantify the value of registered equivalences in frozen prediction tables. The anonymous supplement includes the episode records and independent regrading under `results/structure/`.

K.4 Typed submissions and fixed-observation inference

Submission format. Both matched arms accept complete 64-score prediction objects and record the submitted table as the final artifact. The estimator menu additionally exposes GP fitting and agent-supplied structure rules.

Matched typed-interface episodes. The matched typed and fixed-observation studies were executed on September 25, 2026 (UTC), using API identifier `deepseek-v4-flash`. The prospective study pairs a ridge-only submission interface with a ridge, GP, and agent-rule menu on concrete, wine, astronaut, and SciFact at $B = 20$. Both arms use Flash, the same code-visible task and typed complete-table argument, two free anchors, 20 purchased outcomes, 20 calculation calls, and a 1,800-second deadline. Arm order alternates across sources. Both prompts request a first-call report of inactive-option rules. The menu also exposes `fit_estimator` in numerical Python. Three of four menu trajectories successfully call the rule-aware GP helper during calculation. All eight final calls submit direct tables without estimator or rule parameters.

Both arms deliver 4/4 artifacts and report 6/6 registered rules. Seven of eight tables satisfy every verified equivalence. The paired menu-minus-ridge mean is -0.0923, with one positive and three negative source contrasts. Source-level results appear below.

Source	Ridge R	Menu R	Menu − ridge	Clean tables
Concrete	0.8990	0.9291	$+0.0301$	2/2
Wine	0.4465	0.4455	-0.0010	2/2
Astronaut	0.8865	0.6758	-0.2107	1/2
SciFact	0.6071	0.4194	-0.1877	2/2

Offline common-estimator fits hold each episode's 22 observations fixed. Registered-rule columns use the verified code rules from the frozen plan.

Acquisition arm	Shared D2	D2 + rules	Shared GP	GP + rules
Ridge-only	0.319	0.601	0.509	0.666
Menu	0.224	0.492	0.350	0.535

Fresh inference from fixed observations. Each fresh Flash agent receives the 22 observations from the matched typed ridge-only episode, with zero remaining measurement credits and a 900-second session. The final call requires a named estimator and agent-supplied rules. All four agents report and submit their source's registered rules, covering six registered source-specific relations across the study. Three choose GP and one chooses main-effect ridge. All 96 checked native-equivalent pairs receive identical predictions. The four final tables attain mean recovery 0.682; the separate source-matched typed ridge-only direct tables attain 0.710.

Source	Typed direct R	Fixed R	Estimator	Rules / violations
Concrete	0.899	0.928	GP	2/2, 0/32
Wine	0.446	0.407	GP	1/1, 0/16
Astronaut	0.887	0.767	D1	2/2, 0/32
SciFact	0.607	0.625	GP	1/1, 0/16

The anonymous supplement includes both frozen plans, the typed submissions, intermediate calculations, and final regrading.

K.5 PROSPECTIVE TYPED SOURCE COHORT

The frozen study pairs Flash and Pro on 12 four-factor sources at $B = 8$ under the same typed task and tool interface. Six sources are the paired four/six-factor agent sources; the plan adds the alphabetically first agent-unevaluated source ID in each family before this cohort's model outcomes. Every episode receives two free anchors, up to eight purchased outcomes, 20 numerical calculation calls, and a 1,800-second deadline. The paired source is the aggregation unit. All 24 episodes purchase eight outcomes, and 23 deliver complete tables. The Pro Astronaut episode reaches its session deadline after its eighth purchase without a final table. The first 20 jobs follow the frozen paired launch order. A recorded scheduling amendment runs the final Astronaut and SciFact jobs across sources with four concurrent sessions; tasks, prompts, budgets, estimators, and scoring remain fixed. The amendment is included with the anonymous supplement. The 24 episodes were executed on September 25, 2026 (UTC), using API identifiers `deepseek-v4-flash` and `deepseek-v4-pro`.

Table 4 summarizes source groups, delivery, and inference in the main text. R_{all} assigns zero recovery to a missing final artifact; R_{del} averages delivered artifacts; R_{GP} fits a common GP to the same purchased masks and utilities in every episode. The paired gain is $R_{\mathrm{all}} - R_{\mathrm{GP}}$, with descriptive 2.5th–97.5th percentile source-bootstrap ranges from 20,000 resamples. The GP uses purchased mask–utility pairs; agent tables may also use public workflow code and sandbox calculations.

Flash submits a direct typed prediction table on all 12 sources. Pro submits ten direct tables, selects the named GP on Coffee, and has the one Astronaut non-delivery. The source-level table preserves every attempt. Flash delivers on all 12 sources; Pro delivery is shown explicitly for each source. The Astronaut Pro GP value uses its purchased observations while its R_{all} is zero. D2 GP fits the observations from the frozen pair-effect design for that source.

Source	Group	Flash R	Flash GP	Pro valid	Pro R_{all}	Pro GP	D2 GP
Banknote	New	0.829	0.797	1	0.768	0.623	0.745
Airfoil	New	0.801	0.695	1	0.718	0.691	0.717
Dry Bean	New	0.852	0.637	1	0.853	0.590	0.590
El Niño	New	0.987	0.960	1	0.992	0.981	0.967
Coffee	New	0.881	0.538	1	0.732	0.732	0.732
ArguAna	New	0.861	0.689	1	0.688	0.689	0.709
Spambase	Original	0.562	0.666	1	0.652	0.514	0.560
Concrete	Original	0.922	0.885	1	0.872	0.872	0.885
Wine	Original	0.895	0.713	1	0.901	0.418	0.494
CO_2	Original	0.499	0.437	1	0.245	0.667	0.667
Astronaut	Original	0.894	0.259	0	0.000	0.707	0.584
SciFact	Original	0.811	0.747	1	0.871	0.821	0.821

Across Pro's 11 delivered sources, $R_{\mathrm{del}} = 0.754$ and the GP mean on those same sources is 0.691, giving a delivered-only difference of $+0.063$. The named GP submission on Coffee gives an exact zero difference. The shared-GP acquisition contrast compares agent-purchased observations with the frozen D2 design. On the six new sources its mean is -0.024 for Flash (descriptive source-bootstrap range $[-0.096, 0.029]$) and -0.026 for Pro ($[-0.066, 0.002]$). Across all 12 sources the respective means are -0.037 ($[-0.121, 0.041]$) and -0.014 ($[-0.044, 0.019]$). On the six paired sources, the Flash mean is -0.051, with two positive, one tied, and three negative source contrasts. A post-hoc sensitivity selects the strongest of the same-observation main-effect ridge, pair-effect ridge, and GP fits separately for each source. Flash delivered tables exceed this per-source best fit on all six new sources by 0.114 mean recovery and on 10 of 12 sources overall by 0.095. Pro exceeds it on four new sources, with a six-source mean difference of 0.073. The frozen episode plan, amendment, all 24 attempts, independent regrading, and source-bootstrap analysis appear in the anonymous supplement.

L SENSITIVITY AND ADDITIONAL-WORKFLOW RESULTS

L.1 SENSITIVITY TO INDIVIDUAL SOURCES

Each comparison is paired by source. The original Flash comparison first averages its two trials within each source; the additional comparison uses its separate execution on each source. We report the mean and median recovery change, counts of positive, tied, and negative sources, and the range of paired means after omitting each of the six sources in turn. These ranges describe the composition of the evaluated catalog.

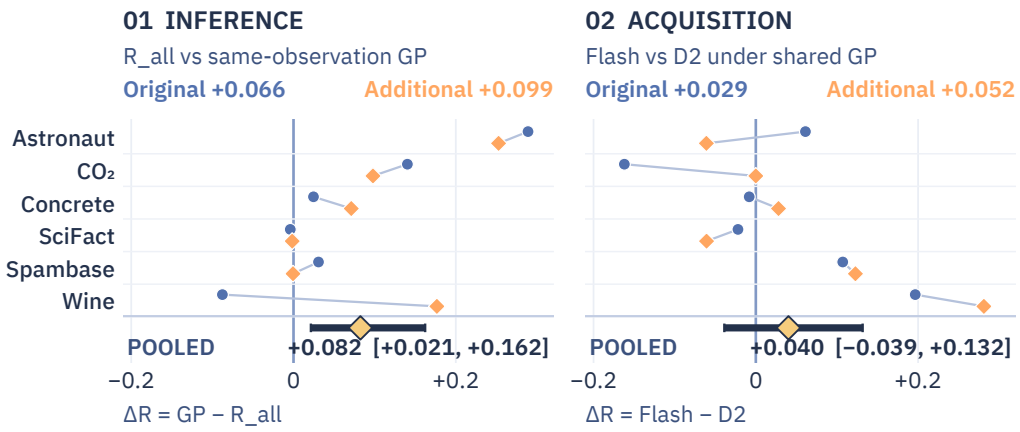

Figure 5: Source-level acquisition and inference contrasts at $B = 8$. Each source has one original-cohort point, averaging two Flash episodes, and one additional-cohort point from one episode. The left panel compares Flash R_{all} with a GP fitted to the same observations. The right panel compares Flash and D2 observations under that GP. Pooled means average cohorts within source; bars are descriptive source-bootstrap percentile ranges from 20,000 resamples.

Comparison	B	Mean ΔR	Median	$+/=/-$	Source omission range	
Shared GP, Flash original	8	+0.066	+0.028	4 / 0 / 2	+0.021	+0.096
Shared GP, Flash additional	8	+0.099	+0.085	4 / 0 / 2	+0.069	+0.120
Code GP-E over GP-E	20	+0.214	+0.166	4 / 2 / 0	+0.121	+0.257
Code D2 over D2	20	+0.233	+0.231	4 / 2 / 0	+0.167	+0.279
Code GP-E over GP-E	32	+0.159	+0.131	4 / 2 / 0	+0.096	+0.191
Code D2 over D2	32	+0.205	+0.136	4 / 2 / 0	+0.113	+0.246

Paired source contrasts. At $B = 8$, each contrast fits the same GP to observations from two acquisition policies or compares that fit with agent R_{all}. Each of the six sources is a resampling cluster. The original cohort first averages its two episodes within source; the additional cohort has one episode per source. Pooled contrasts average the two cohort contrasts within source, retaining six source-level resampling units. Descriptive percentile ranges use 20,000 source-bootstrap resamples. The final column counts positive, tied, and negative sources.

Flash cohort	Paired contrast	Mean ΔR	Source bootstrap range	$+/=/-$
Original	GP $-R_{\text{all}}$	+0.066	$[-0.021, +0.167]$	4/0/2
Original	GP − D2	+0.029	$[-0.064, +0.115]$	3/0/3
Original	GP − GP-E	+0.058	$[-0.046, +0.164]$	4/0/2
Additional	GP $-R_{\text{all}}$	+0.099	$[+0.028, +0.172]$	4/0/2
Additional	GP − D2	+0.052	$[-0.031, +0.155]$	3/1/2
Additional	GP − GP-E	+0.081	$[-0.023, +0.202]$	3/1/2
Pooled	GP $-R_{\text{all}}$	+0.082	$[+0.021, +0.162]$	5/0/1
Pooled	GP − D2	+0.040	$[-0.039, +0.132]$	4/0/2
Pooled	GP − GP-E	+0.069	$[-0.029, +0.180]$	3/0/3

The pooled Flash gain from shared GP over delivery is $+0.082$, with a descriptive source-bootstrap range of $[+0.021, +0.162]$. GP fitted to Flash observations also has higher six-source means than GP fitted to D2 or GP-E observations in both cohorts. Their source-bootstrap ranges show variation across acquisition policies. The original shared-GP mean advantage ranges from 0.021 to 0.096 under source omission. The additional Flash cohort has a mean gain of 0.099, with a source-omission range of 0.069 to 0.120. Four sources improve and two decline in each cohort. Program-equivalence controls improve on all four sources with nontrivial classes. Classification and forecasting retain identity maps and yield the same predictions as their corresponding controls. At both reported budgets, every source-omission mean remains positive. The anonymous supplement includes all per-source contrasts and source-omission means.

L.2 Strict-error tolerances

Each row summarizes five tolerances on the same saved predictions. Track four uses all 22 four-factor sources; track six uses the six paired sources. Strict counts use maximum conditional-effect error relative to the response range. Exact is the number of optimal configuration choices, and the final column averages recovery among those exact-choice cases.

Track	Method	B	N	Strict count at tolerance τ					Exact	$R \mid$ Exact
				.025	.05	.10	.20	.40		
4 factors	D1	8	22	0	1	1	5	13	15	0.618
4 factors	D2	8	22	1	1	3	8	20	15	0.634
4 factors	GP-G	8	22	1	1	2	10	19	15	0.669
4 factors	GP-E	8	22	1	1	1	12	19	16	0.717
6 factors	D1	8	6	0	0	0	0	1	2	0.405
6 factors	D2	8	6	0	0	0	0	0	0	–
6 factors	GP-G	8	6	0	0	0	1	1	0	–
6 factors	GP-E	8	6	0	0	0	0	2	0	–
6 factors	Code D1	8	6	0	0	0	1	1	2	0.063
6 factors	Code D2	8	6	0	0	0	0	0	1	0.000
6 factors	Code GP-E	8	6	0	0	0	1	1	2	0.544
6 factors	D1	32	6	0	0	0	1	2	2	0.431
6 factors	D2	32	6	0	0	1	1	2	2	0.598
6 factors	GP-G	32	6	0	0	1	1	4	2	0.682
6 factors	GP-E	32	6	0	0	1	1	4	2	0.704
6 factors	Code D1	32	6	0	2	2	3	3	3	0.786
6 factors	Code D2	32	6	1	1	3	3	3	2	0.987
6 factors	Code GP-E	32	6	1	2	2	3	4	3	0.925

This profile connects the continuous metric to several maximum-error criteria. For example, D2 at $B = 8$ passes on 3/22 sources at the 10% tolerance and 8/22 at 20%, while its 15 exact choices remain the same. Native-case response scales appear in Appendix E.

L.3 Magnitude of conditional reversals

A reversal requires at least one positive and one negative background effect whose magnitudes both exceed the indicated floor. Source counts merge paired dimensional variants. The two largest floors identify substantial conditional changes within the fixed response range.

Effect floor	Components / 172	Conditions / 36	Sources / 30
10^{-12} utility	121	35	29
1% of response range	98	33	28
5% of response range	59	24	20
10% of response range	31	16	14

L.4 NATIVE-UNIT SENSITIVITY

The analysis applies the inverse utility map to saved predictions and computes effects in native units. Fitted models and observed sets remain fixed. All 3,246 analysed original control records have finite inverses. Raw native errors are reported by source in the anonymous supplement, preserving each source's units. The table compares family-macro recovery at the main four-factor budget and both reported paired budgets. N counts sources. Native strict counts successful records across all seeds, with 20 seeds for each random design.

Track	Method	B	N	Utility R	Native R	Native strict
4 factors	D1	8	22	0.571	0.562	1/22
4 factors	D2	8	22	0.612	0.633	3/22
4 factors	Random D2	8	22	0.503	0.505	14/440
4 factors	GP-G	8	22	0.661	0.669	2/22
4 factors	GP-E	8	22	0.701	0.712	2/22
6 factors	D1	20	6	0.192	0.197	0/6
6 factors	D2	20	6	0.157	0.171	0/6
6 factors	Random D2	20	6	0.214	0.216	0/120
6 factors	GP-G	20	6	0.330	0.334	0/6
6 factors	GP-E	20	6	0.248	0.252	0/6
6 factors	Code D1	20	6	0.303	0.296	1/6
6 factors	Code D2	20	6	0.389	0.384	1/6
6 factors	Code GP-E	20	6	0.462	0.468	1/6
6 factors	D1	32	6	0.298	0.301	0/6
6 factors	D2	32	6	0.445	0.451	1/6
6 factors	Random D2	32	6	0.465	0.466	17/120
6 factors	GP-G	32	6	0.548	0.547	1/6
6 factors	GP-E	32	6	0.537	0.538	1/6
6 factors	Code D1	32	6	0.545	0.545	2/6
6 factors	Code D2	32	6	0.650	0.650	3/6
6 factors	Code GP-E	32	6	0.697	0.697	2/6

At four factors and $B = 8$, D2 recovery is 0.612 in utility units and 0.633 in native units; GP-E gives 0.701 and 0.712. The paired code-equivalence gains also persist under this transformation. These comparisons describe the effect of utility normalization on the reported reconstructions.

L.5 SIGNAL AND GRAPH WORKFLOWS

Figure 6 and the source profiles describe all eight added six-factor cases. Order ≥ 3 variance is the uniform-cube Fourier share from interactions of order three or higher (O'Donnell, 2014). Curves average seeds within source, then sources within family.

Source	Min	Max	Sign reversals	Order ≥ 3 variance
mitdb_100	0.502	1.000	4	0.162
mitdb_101	0.369	0.996	6	0.140
mitdb_102	0.554	1.000	5	0.386
mitdb_103	0.506	1.000	5	0.153
graph_lesmis	0.500	0.903	6	0.419
graph_adjnoun	0.500	0.747	5	0.084
graph_football	0.500	0.892	5	0.265
graph_dolphins	0.500	0.764	6	0.432

At $B = 20$, two-family recovery is 0.0439 for pair ridge and 0.0435 for GP-E. The complete controls cover all methods, budgets, and random seeds through full enumeration.

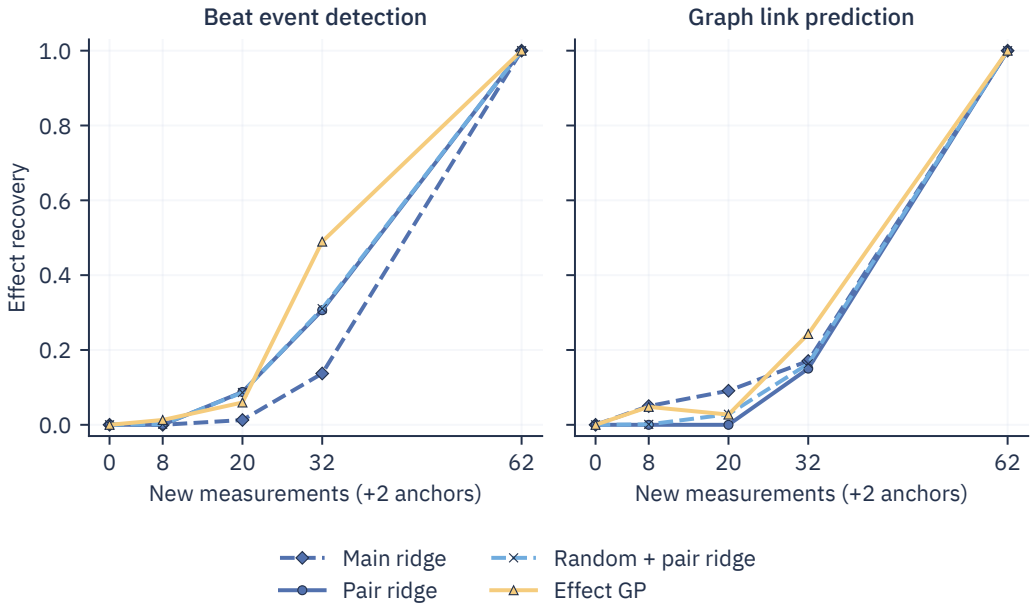

Figure 6: Recovery across measurement budgets for beat detection and link prediction. Each family contains four source instances, with complete native references and the same experimental-design and reconstruction interfaces.

L.6 Completed agent predictions on the added families

The frozen eight-source extension attempts four beat-detection and four graph tasks at $B = 32$. Six episodes deliver tables, covering three sources in each family. The other sources are MIT-BIH record 103 and graph dolphins; they have purchased observations and no submitted prediction table. The table compares each submission with same-observation GP and source-matched D2, grid-GP, and effect-GP controls.

Family	Source	Agent R	Shared GP	D2	GP-G	GP-E
Beat detection	mitdb_100	0.480	0.624	0.279	0.356	0.533
Beat detection	mitdb_101	0.515	0.642	0.336	0.509	0.536
Beat detection	mitdb_102	0.242	0.452	0.178	0.213	0.383
Beat detection mean		0.412	0.573	0.264	0.359	0.484
Link prediction	graph_lesmis	0.000	0.185	0.000	0.467	0.000
Link prediction	graph_adjnoun	0.528	0.596	0.425	0.591	0.565
Link prediction	graph_football	0.053	0.234	0.163	0.348	0.406
Link prediction mean		0.194	0.338	0.196	0.469	0.324
Six-source macro		0.303	0.455	0.230	0.414	0.404

Shared GP improves all six delivered tables. Their family-macro recovery rises from 0.303 to 0.455, with beat and graph gains of 0.160 and 0.145. The all-attempt R_{all} values across four sources per family are 0.309 for beat detection, 0.145 for graph prediction, and 0.227 with equal family weight. The anonymous supplement retains the frozen plan and eight-attempt ledger.

Graph code-equivalence diagnostic. All four frozen graph references give identical native predictions and scores for masks `000000` and `000001`. A CPU diagnostic applies this relation to three completed $B = 32$ submissions. Setting the second mask to the measured first-mask score raises mean submitted recovery from 0.194 to 0.312; canonicalizing the pair for same-observation GP raises recovery from 0.338 to 0.516. Projection improves two submissions and GP all three. The anonymous supplement contains the native and prediction audits.